

CLOUDS, GRAVITY AND METALLICITY IN BLUE L DWARFS: THE CASE OF 2MASS J11263991–5003550⁸

ADAM J. BURGASSER^{1,2}, DAGNY L. LOOPER^{2,3}, J. DAVY KIRKPATRICK⁴, KELLE L. CRUZ^{5,6}, AND BRANDON J. SWIFT^{3,7}

Accepted for publication to ApJ

ABSTRACT

Optical and near-infrared spectroscopy of the newly discovered peculiar L dwarf 2MASS J11263991–5003550 are presented. Folkes et al. identified this source as a high proper motion L9±1 dwarf based on its strong H₂O absorption at 1.4 μm. We find that the optical spectrum of 2MASS J1126–5003 is in fact consistent with that of a normal L4.5 dwarf with notably enhanced FeH absorption at 9896 Å. However, its near-infrared spectrum is unusually blue, with strong H₂O and weak CO bands similar in character to several recently identified “blue L dwarfs”. Using 2MASS J1126–5003 as a case study, and guided by trends in the condensate cloud models of Burrows et al. and Marley et al., we find that the observed spectral peculiarities of these sources can be adequately explained by the presence of thin and/or large-grained condensate clouds as compared to normal field L dwarfs. Atypical surface gravities or metallicities alone cannot reproduce the observed peculiarities, although they may be partly responsible for the unusual condensate properties. We also rule out unresolved multiplicity as a cause for the spectral peculiarities of 2MASS J1126–5003. Our analysis is supported by examination of *Spitzer* mid-infrared spectral data from Cushing et al. which show that bluer L dwarfs tend to have weaker 10 μm absorption, a feature tentatively associated with silicate oxide grains. With their unique spectral properties, blue L dwarfs like 2MASS J1126–5003 should prove useful in studying the formation and properties of condensates and condensate clouds in low temperature atmospheres.

Subject headings: stars: atmospheres — stars: fundamental parameters — stars: individual (2MASS J11263991–5003550) — stars: low mass, brown dwarfs

1. INTRODUCTION

L dwarfs comprise one of the two latest-type spectral classes of very low mass stars and brown dwarfs, spanning masses at and below the hydrogen burning minimum mass (see Kirkpatrick 2005 and references therein). They are inexorably linked to the presence and properties of liquid and solid condensates which form in their cool photospheres (e.g., Tsuji, Ohnaka, & Aoki 1996; Burrows & Sharp 1999; Ackerman & Marley 2001; Allard et al. 2001; Cooper et al. 2003; Tsuji 2005). These condensates significantly influence the spectral energy distributions and photospheric gas abundances of L dwarfs, by removing gaseous TiO and VO from the photosphere and enabling the retention of atomic alkali species (e.g., Fegley & Lodders 1996; Burrows & Sharp 1999; Lodders 2002). Weakened H₂O absorption through backwarming effects (e.g.,

Jones & Tsuji 1997; Allard et al. 2001) and red near-infrared colors ($J - K \approx 1.5$ –2.5; Kirkpatrick et al. 2000) also result from condensate opacity. In addition, periodic and aperiodic photometric variability observed in several L dwarfs has been associated with surface patchiness in photospheric condensate clouds (e.g., Bailer-Jones & Mundt 1999, 2001; Gelino et al. 2002; Mohanty et al. 2002). Condensate abundances at the photosphere appear to reach their zenith amongst the mid- and late-type L dwarfs (Kirkpatrick et al. 1999; Chabrier et al. 2000; Ackerman & Marley 2001) before disappearing from the photospheres of cooler T dwarfs (Marley et al. 1996; Tsuji et al. 1996; Allard et al. 2001; Cushing et al. 2006). The abundances of photospheric condensates, their grain size distribution, and the radial and surface structure of condensate clouds may vary considerably from source to source, as well as temporally for any one source, and the dependencies of these variations on various physical parameters are only beginning to be explored (Helling et al. 2001; Woitke & Helling 2003; Knapp et al. 2004).

With hundreds of L dwarfs now known,⁹ groupings of peculiar L dwarfs – sources whose spectral properties diverge consistently from the majority of field objects – are becoming distinguishable. Examples include young, low surface gravity brown dwarfs (McGovern et al. 2004; Kirkpatrick et al. 2006; Allers et al. 2007; Cruz et al. 2007) and metal-poor L subdwarfs (Burgasser et al. 2003a; Lépine, Rich, & Shara 2003; Gizis & Harvin 2006; Burgasser, Cruz & Kirkpatrick 2007). There also exists a class of peculiar “blue” L dwarfs (Cruz et al.

¹ Massachusetts Institute of Technology, Kavli Institute for Astrophysics and Space Research, Building 37, Room 664B, 77 Massachusetts Avenue, Cambridge, MA 02139; ajb@mit.edu

² Visiting Astronomer at the Infrared Telescope Facility, which is operated by the University of Hawaii under Cooperative Agreement NCC 5-538 with the National Aeronautics and Space Administration, Office of Space Science, Planetary Astronomy Program.

³ Institute for Astronomy, University of Hawaii, 2680 Woodlawn Drive, Honolulu, HI 96822

⁴ Infrared Processing and Analysis Center, M/S 100-22, California Institute of Technology, Pasadena, CA 91125

⁵ Astronomy Department, California Institute of Technology, Pasadena, CA 91125

⁶ NSF Astronomy and Astrophysics Postdoctoral Fellow

⁷ Currently at Steward Observatory, University of Arizona, 933 N. Cherry Ave., Tucson, AZ 85721

⁸ This paper includes data gathered with the 6.5 meter Magellan Telescopes located at Las Campanas Observatory, Chile.

⁹ A current list is maintained at <http://dwarfarchives.org>.

2003, 2007; Knapp et al. 2004), roughly a dozen sources exhibiting normal optical spectra but unusually blue near-infrared colors and strong near-infrared H₂O, FeH and K I features. Various studies have attributed these peculiarities to subsolar metallicity, high surface gravity, unresolved multiplicity and peculiar cloud properties (Gizis et al. 2000; Cruz et al. 2003, 2007; McLean et al. 2003; Burgasser et al. 2004; Knapp et al. 2004; Chiu et al. 2006; Folkes et al. 2007). Any one of these characteristics may impact the presence and character of condensates and condensate clouds in low temperature atmospheres.

In an effort to identify new nearby and peculiar L dwarfs, we have been searching for late-type dwarfs using near-infrared imaging data from the Deep Near Infrared Survey of the Southern Sky (DENIS; Epchtein et al. 1997). One of the objects identified in this program is DENIS J112639.9–500355, a bright source which was concurrently discovered by Folkes et al. (2007) in the SuperCOSMOS Sky Survey (Hambly et al. 2001a,b,c, hereafter SSS) and the Two Micron All Sky Survey (hereafter 2MASS; Skrutskie et al. 2006). It is designated 2MASS J11263991–5003550 in that study, and we refer to the source hereafter as 2MASS J1126–5003. Based on its blue near-infrared colors and deep H₂O absorption bands, Folkes et al. (2007) concluded that 2MASS J1126–5003 is a very late-type L dwarf (L9±1) which may have unusually patchy or thin condensate clouds. In this article, we critically examine the observational properties of 2MASS J1126–5003 to unravel the origins of its spectral peculiarities, and examine it as a representative of the blue L dwarf subgroup.

Our identification of 2MASS J1126–5003 and a slightly revised determination of its proper motion using astrometry from the SSS, DENIS and 2MASS catalogs are described in § 2. Optical and near-infrared spectroscopic observations and their results are described in § 3, along with determination of the optical and near-infrared classifications of 2MASS J1126–5003 and estimates of its distance and space kinematics. In § 4 we analyze the properties of 2MASS J1126–5003 and blue L dwarfs in general, considering metallicity, surface gravity, condensate cloud and unresolved multiplicity effects. We also introduce a new near-infrared H₂O index that eliminates discrepancies between optical and near-infrared types for these sources. Results are discussed and summarized in § 5.

2. IDENTIFICATION OF 2MASS J1126–5003

We initially identified 2MASS J1126–5003 in the DENIS Data Release 3 point source catalog as part of a sample constrained to have $9 \leq J \leq 15.5$, $I - J \geq 3$ (corresponding to spectral types M8 and later), $J - K_s \leq 2.8$ (to exclude background giants), galactic latitudes $|b| \geq 8^\circ$ (excluding the Galactic plane) and declinations $-90^\circ \leq \delta \leq +2^\circ$. Further details on this search sample and resulting discoveries will be made in a future publication (D.Looper et al., in preparation). The combined DENIS and 2MASS colors of 2MASS J1126–5003 are $I - J = 3.80 \pm 0.15$ and $J - K_s = 1.17 \pm 0.04$, consistent with a late type star or brown dwarf (e.g., Delfosse et al. 1997; Kirkpatrick et al. 2000).

Figure 1 displays optical field images centered on the 2MASS/DENIS coordinates of 2MASS J1126–5003 as

observed by the ESO *R* (epoch 1983 February 14 UT), SERC *I_N* (epoch 1985 March 14 UT) and AAO *R* (epoch 1992 March 28 UT) photographic plate surveys (e.g., Hartley & Dawe 1981; Cannon 1984). There are no optical counterparts to 2MASS J1126–5003 in these images at the exact 2MASS/DENIS position, but faint, offset counterparts can be discerned. Based on SSS and 2MASS astrometry spanning 14.2 yr, Folkes et al. (2007) determined a substantial proper motion for 2MASS J1126–5003, $\mu = 1''.65 \pm 0''.03 \text{ yr}^{-1}$. We confirm that the faint *R*-band (20.4 mag) and *I_N*-band (17.6 mag¹⁰) counterparts in the 1983 and 1985 photographic plate images are at the expected position of 2MASS J1126–5003 based on this motion, neither of which have coincident near-infrared counterparts.¹¹ The associated optical/near-infrared colors ($R_{ESO} - J = 6.4$; $I_N - J = 3.6$) are again indicative of a late-type dwarf. A linear fit to the SSS, DENIS and 2MASS astrometry over 16.3 yr (Table 1) yields a value of $\mu = 1''.66 \pm 0''.03 \text{ yr}^{-1}$ at position angle $\theta = 285^\circ 3 \pm 1^\circ 6$, where uncertainties include an estimated 0''.3 astrometric uncertainty in both Right Ascension and declination for all three catalogs. Not surprisingly, this value is consistent with the measurement of Folkes et al. (2007). Note that neither proper motion measurement takes into account parallactic reflex motion, which is presumably much smaller than the aggregate linear motion of 2MASS J1126–5003 since 1983 (nearly 30'').

3. SPECTROSCOPIC OBSERVATIONS

3.1. Optical Data

Optical spectroscopy of 2MASS J1126–5003 was obtained on 2006 May 8 (UT) using the Low Dispersion Survey Spectrograph (LDSS-3) mounted on the Magellan 6.5m Clay Telescope. LDSS-3 is an imaging spectrograph, upgraded from the original LDSS-2 (Allington-Smith et al. 1994) for improved red sensitivity. Conditions during the observations were clear with moderate seeing (0''.7 at *R*-band). We employed the VPH-red grism (660 lines/mm) with a 0''.75 (4 pixels) wide longslit mask, aligned to the parallactic angle, to acquire 6050–10500 Å spectra across the entire chip with an average resolution of $\lambda/\Delta\lambda \approx 1800$. Dispersion along the chip was 1.2 Å/pixel. The OG590 longpass filter was used to eliminate second order light shortward of 6000 Å. A single slow-read exposure of 750 s was obtained at an airmass of 1.08. We also observed the G2 V star HD 97625 immediately after the 2MASS J1126–5003 observation and at a similar airmass for telluric absorption correction. The flux standard LTT 7987 (a.k.a. GJ 2147; Hamuy et al. 1994) was observed during the same run on 2006 May 7 (UT) using an identical slit and grism combination. All spectral observations were accompanied by HeNeAr arc lamp and flat-field quartz lamp exposures for dispersion and pixel response calibration.

LDSS-3 data were reduced in the IRAF¹² environ-

¹⁰ Optical photometry as given in the SSS.

¹¹ A brighter optical star is coincident with the motion-corrected position of 2MASS J1126–5003 in the 1992 AAO *R* image and obscures the proper motion source.

¹² IRAF is distributed by the National Optical Astronomy Observatories, which are operated by the Association of Universities for Research in Astronomy, Inc., under cooperative agreement with

ment. Raw science images (separated into short and long wavelength halves) were first trimmed and subtracted by a median combined set of slow-read bias frames taken during the afternoon. The resulting images were then divided by the corresponding normalized, median-combined and bias-subtracted set of flat field frames. The G star spectra were first extracted using the APALL task, utilizing background subtraction and optimal extraction options. The spectrum of 2MASS J1126–5003 was extracted using the G star dispersion trace as a template. Dispersion solutions were determined from the arc lamp spectra extracted using the same dispersion trace; solutions were accurate to ~ 0.1 pixels, or ~ 0.12 Å. Flux calibration was determined using the tasks STANDARD and SENSFUNC with observations of LTT 7987, adequate over the spectral range 6000–10000 Å. Corrections to telluric O₂ (6860–6960 Å B-band, 7580–7700 Å A-band) and H₂O (7150–7300 Å) absorption bands were determined by linearly interpolating over these features in the G dwarf spectrum, dividing by the uncorrected spectrum, and multiplying the result with the spectrum of 2MASS J1126–5003. Note that we did not correct for 9270–9675 Å telluric H₂O absorption due to the reduced signal at these wavelengths in the target and G dwarf spectra. Short and long wavelength data were then stitched together with no additional flux scaling.

The reduced red optical spectrum of 2MASS J1126–5003 is shown in Figure 2, compared to the L4.5 2MASS J22244381-0158521 (Kirkpatrick et al. 2000, hereafter 2MASS J2224-0158) and the L5 2MASS J1507476-162738 (Reid et al. 2000, hereafter 2MASS J1507-1627)¹³. The overall optical spectral morphology of 2MASS J1126–5003 is well-matched to both L dwarf comparison sources, agreeing best with the L4.5 shortward of the pressure-broadened 7665/7699 Å K I doublet (Burrows, Marley, & Sharp 2000; Allard et al. 2003; Burrows & Volobuyev 2003) and the L5 longward of this feature. 2MASS J1126–5003 exhibits the same peak-up in flux between the blue wing of K I and the red wing of the pressure-broadened 5890/5896 Å Na I D lines present in the L dwarf comparison spectra, as well as line absorption from Rb I (7800 and 7948 Å), Na I (8183/8195 Å doublet) and Cs I (8521 Å). These lines are shown in detail in Figure 3, and their equivalent widths (EW) are listed in Table 2. Line strengths are similar to those of other midtype field L dwarfs (Kirkpatrick et al. 1999). The optical spectrum of 2MASS J1126–5003 also exhibits strong metal hydride bands at 6950 Å (CaH), 8600 Å (CrH and FeH) and 9896 Å (FeH); and weak TiO absorption at 7100 and 8400 Å. The 9896 Å Wing-Ford band of FeH is clearly stronger in the spectrum of 2MASS J1126–5003 as compared to either of the L dwarf comparison sources, while the 8400 Å TiO is also slightly deeper, particularly in

contrast to 2MASS J1507-1627. These features suggest that 2MASS J1126–5003 could be slightly metal-poor, exhibiting the same peculiarities as L subdwarfs (Burgasser et al. 2003a; Burgasser, Cruz & Kirkpatrick 2007), a point that is discussed further in § 4.2.2.

A close examination at the 6500–6750 Å region (inset in Figure 2) reveals no significant emission from the 6563 Å H α line, an indicator of magnetic activity. The absence of H α is consistent with the general decline in optical magnetic emission between late-type M to mid-type L dwarfs (Gizis et al. 2000; Mohanty & Basri 2003; West et al. 2004). There is a weak feature at the location of the 6708 Å Li I line, an indicator of substellar mass (Rebolo, Martín, & Magazzu 1992), but is of the same strength as noise features in this spectral region. The upper limit EW of the Li I line (< 0.4 Å) is considerably less than the minimum measured EWs of detected lines in other L-type brown dwarfs (~ 3 Å; Kirkpatrick et al. 2000). We therefore conclude that Li I absorption is not present in the spectrum of 2MASS J1126–5003, although higher resolution, higher signal-to-noise observations are necessary to confirm this result.

3.2. Near-Infrared Data

Low resolution near-infrared spectral data for 2MASS J1126–5003 were obtained in clear conditions on 2006 December 20 (UT) using the SpeX spectrograph (Rayner et al. 2003) mounted on the 3m NASA Infrared Telescope Facility (IRTF). The 0.5 slit was employed, providing 0.75–2.5 μm spectroscopy with resolution $\lambda/\Delta\lambda \approx 120$ and dispersion across the chip of 20–30 Å pixel⁻¹. To mitigate the effects of differential refraction, the slit was aligned to the parallactic angle. Due to the southern declination of this source, observations were made close to transit but at fairly high airmass (3.0). 12 exposures of 60 s each were obtained in an ABBA dither pattern along the slit. The A0 V star HD 101802 was observed immediately afterward at a similar airmass (3.1) for flux calibration. Internal flat field and Ar arc lamps were also observed for pixel response and wavelength calibration.

Data were reduced using the SpeXtool package, version 3.3 (Cushing, Vacca, & Rayner 2004), using standard settings. Raw science images were first corrected for linearity, pair-wise subtracted, and divided by the corresponding median-combined flat field image. Spectra were optimally extracted using the default settings for aperture and background source regions, and wavelength calibration was determined from arc lamp and sky emission lines. The multiple spectral observations were then median-combined after scaling individual spectra to match the highest signal-to-noise observation. Telluric and instrumental response corrections for the science data were determined using the method outlined in Vacca et al. (2003), with line shape kernels derived from the arc lines. Adjustments were made to the telluric spectra to compensate for differing H I line strengths in the observed A0 V spectrum and pseudo-velocity shifts. Final calibration was made by multiplying the spectrum of 2MASS J1126–5003 by the telluric correction spectrum, which includes instrumental response correction through the ratio of the observed A0 V spectrum to a

the National Science Foundation.

¹³ The optical spectra of 2MASS J2224-0158 and 2MASS J1507-1627 were obtained using the Low Resolution Imaging Spectrograph (LRIS, Oke et al. 1995) mounted on the Keck 10m Telescope, and reduced by J. D. Kirkpatrick using identical IRAF routines. Comparisons of late-type spectra observed with both instruments show consistency to within 10% over the 6100–9000 Å range (Burgasser, Cruz & Kirkpatrick 2007).

scaled, shifted and deconvolved Kurucz¹⁴ model spectrum of Vega.

The reduced spectrum of 2MASS J1126–5003 is shown in Figure 4 and compared to equivalent SpeX prism data for 2MASS J2224-0158 (K. Cruz et al., in preparation) and 2MASS J1507-1627 (Burgasser 2007b). While all three spectra exhibit features in common, including strong H₂O (1.4 and 1.9 μm), CO (2.3 μm) and FeH bands (0.99, 1.2 and 1.6 μm), and line absorption from K I and Na I in the 1.1–1.25 μm region, overall spectral morphologies differ markedly. The near-infrared spectrum of 2MASS J1126–5003 is a better match to that of 2MASS J1507-1627, but is clearly bluer than both L dwarf comparison sources. This is consistent with its bluer near-infrared colors, $J - K_s = 1.17 \pm 0.04$ versus 2.05 ± 0.04 and 1.52 ± 0.04 for 2MASS J2224-0158 and 2MASS J1507-1627, respectively.¹⁵ 2MASS J1126–5003 also exhibits stronger H₂O absorption and weaker FeH and CO absorption longward of 1.4 μm , although the strong 0.99 μm FeH band is again evident. The deep H₂O band at 1.4 μm was explicitly noted by Folkes et al. (2007) and cited as evidence that this source is a very late-type L dwarf. Indeed, we confirm that only L9 to T1 dwarfs have comparably strong H₂O absorption (see Figure 2 in Folkes et al. 2007), although the absence of 1.6 and 2.2 μm CH₄ absorption bands implies that 2MASS J1126–5003 is not a T dwarf (Burgasser et al. 2002; Geballe et al. 2002). Folkes et al. (2007) also note relatively strong alkali line absorption in the 1.1–1.3 μm spectrum of 2MASS J1126–5003, unresolved in our SpeX prism data.

Differences in the near-infrared spectral morphologies of L dwarfs with similar optical classifications but different $J - K_s$ colors has been previously noted and discussed in the literature (e.g., Fig. 24 in McLean et al. 2003 and Fig. 8 in Burgasser et al. 2007). The spectral comparisons in Figures 2 and 4 serve to emphasize that these differences are largely restricted to near-infrared wavelengths, involving not just shifts in spectral color but in specific features as well. The underlying physical causes for these differences, particularly for blue L dwarfs, are discussed further in § 4.2.

3.3. Spectral Classification

Comparison of the optical spectrum of 2MASS J1126–5003 to those of 2MASS J2224-0158 and 2MASS J1507-1627 in Figures 2 indicate a midtype L dwarf optical classification. A more quantitative determination can be made by measuring the spectral ratios defined by Kirkpatrick et al. (1999). These values are listed in Table 3,¹⁶ and yield an average subtype of $L4.5 \pm 0.5$. Spectral ratios from Martín et al. (1999) and Hawley et al. (2002) were also examined and yield consistent classifications of L4–L5 on the Kirkpatrick et al. (1999) scheme. The consistency of these various indices, and the overall agreement between the spectra of

2MASS J1126–5003 and 2MASS J2224-0158 as shown in Figure 2, indicate a robust optical type of L4.5 for this source.

This classification disagrees significantly with the near-infrared type determined by Folkes et al. (2007), L9 \pm 1, which is based largely on the strength of the deep 1.4 μm H₂O band. This study also noted a “duality” in the near-infrared characteristics of 2MASS J1126–5003, with FeH features at 0.99 and 1.2 μm consistent with an early- to midtype L dwarf (based on indices defined by McLean et al. 2003). As the Folkes et al. (2007) spectrum spanned only the 1.0–1.6 μm region, we re-examined the near-infrared type for this source using our broadband 1.0–2.5 μm SpeX data.

There is as yet no formal spectral classification scheme for L dwarfs in the near-infrared; however, several studies have developed spectral index relations linked to optical classifications. We examined spectral ratios for low-resolution near-infrared data defined by Tokunaga & Kobayashi (1999); Reid et al. (2001); Geballe et al. (2002); Burgasser et al. (2006a); and Allers et al. (2007), which sample the prominent H₂O bands and details within the spectral flux peaks. Values and associated spectral types (based on polynomial relations determined in the studies listed above) are listed in Table 3. We derive an overall near-infrared spectral type of $L6.5 \pm 2$ based on the spectral type/index relations of Reid et al. (2001), with the uncertainty indicating the scatter in the index subtypes. This classification, while formally consistent with that of Folkes et al. (2007), is clearly poorly constrained. If only the indices sampling the 1.4 μm H₂O band are considered, an average type of L8 \pm 1 is derived, in closer agreement with the result of Folkes et al. (2007). However, indices sampling features at wavelengths longward of 1.6 μm (i.e., K1, CH₄ 2.2 μm and CH₄-K) yield a mean type of $L5 \pm 0.5$, consistent with the optical classification and in sharp disagreement with the H₂O indices. The large discrepancy amongst the index subtypes simply reflects the fact that none of the L dwarf spectral standards provide a good match to the near-infrared spectral energy distribution of 2MASS J1126–5003. In other words, its near-infrared spectrum is truly peculiar.

3.4. Estimated Distance and Kinematics

Given its apparently robust optical spectral type, we chose to estimate the properties of 2MASS J1126–5003 by comparing it to other optically-classified midtype L dwarfs. A spectrophotometric distance estimate was determined by comparing this source’s 2MASS JHK_s photometry to seven absolute magnitude/spectral type relations from Dahn et al. (2002); Cruz et al. (2003); Tinney, Burgasser, & Kirkpatrick (2003); and Vrba et al. (2004). The average distance derived was 15 ± 2 pc, which includes a ± 0.5 subclass uncertainty in the optical classification. Distance estimates from J -band photometry (14 pc) were slightly less than those from K_s -band photometry (17 pc), consistent with the blue near-infrared colors of this source relative to other L4–L5 dwarfs. Our estimated distance for 2MASS J1126–5003 is nearly twice that of Folkes et al. (2007) based on their L9 near-infrared type. Given the better agreement in optical spectral morphology between 2MASS J1126–5003 and other L4–L5 dwarfs, we contend

¹⁴ See <http://kurucz.harvard.edu/stars.html>.

¹⁵ We confirmed that the flux calibration of the spectral data for both sources was accurate by computing synthetic colors using 2MASS J and K_s relative spectral response curves from Cohen, Wheaton & Megeath (2003). The synthetic colors agreed with photometric measurements to within their uncertainties.

¹⁶ Note that spectral ratio measurements were made after shifting the spectrum to its frame of rest; see § 3.4.

that our larger distance estimate is likely to be more accurate, assuming that 2MASS J1126–5003 is single (see § 4.2.1).

The estimated distance and measured proper motion for 2MASS J1126–5003 implies a substantial tangential velocity, $V_{tan} = 117 \pm 15$ km s⁻¹. This is one of the highest V_{tan} s estimated or measured for any field L dwarf,¹⁷ surpassed only by the blue L3 dwarf 2MASSI J1721039+334415 (Cruz et al. 2003, hereafter 2MASS J1721+3344) with $V_{tan} = 139 \pm 15$ km s⁻¹ (Schmidt et al. 2007). Indeed, only five out of ~ 150 field L dwarfs with V_{tan} determinations have values greater than 100 km s⁻¹, including 2MASS J1126–5003 (Schmidt et al. 2007, and references therein).

The radial velocity (V_{rad}) of 2MASS J1126–5003 was measured using the Na I, Rb I and Cs I lines present in the 7800–8600 Å region (Figure 3). Line centers were determined from Gaussian fits to the line cores and compared to vacuum wavelengths listed in the Kurucz Atomic Line Database¹⁸ (Kurucz & Bell 1995). The mean and standard deviation of velocity shifts for these five lines gives $V_{rad} = 46 \pm 9$ km s⁻¹, which includes a 5 km s⁻¹ uncertainty in the dispersion solution of the optical data. The corresponding $[U, V, W]$ space velocities of 2MASS J1126–5003 in the Local Standard of Rest (LSR), assuming an LSR solar motion of $[U_{\odot}, V_{\odot}, W_{\odot}] = [10, 5, 7]$ km s⁻¹ (Dehnen & Binney 1998), is estimated as $[85, -98, -6]$ km s⁻¹. These values are just within the 3σ velocity dispersion sphere of local disk M dwarfs ($[\sigma_U, \sigma_V, \sigma_W] \approx [40, 28, 19]$ km s⁻¹ centered at $[-13, -23, -7]$ km s⁻¹; Hawley, Gizis, & Reid 1996), indicating that 2MASS J1126–5003 is likely to be an old disk or thick disk star. 2MASS J1126–5003 would appear to be considerably older than the average field L dwarf. This is consistent with the absence of Li I absorption in its optical spectrum, implying an age $\gtrsim 2$ Gyr for a mass $> 0.065 M_{\odot}$, assuming a best guess $T_{eff} \approx 1700$ K (typical for L4–L5 dwarfs; Golimowski et al. 2004; Vrba et al. 2004) and solar metallicity evolutionary models (Burrows et al. 1997). Table 4 summarizes the estimated physical properties of 2MASS J1126–5003.

4. ANALYSIS

4.1. 2MASS J1126–5003 in Context: The Blue L Dwarfs

The discrepancies between the optical and near-infrared spectral classifications of 2MASS J1126–5003, and the near-infrared spectral peculiarities noted in § 3.2, are consistent with the characteristics of blue L dwarfs reported in the literature. This is illustrated in Figure 5, which compares the optical and near-infrared spectra of 2MASS J1126–5003 and three early-type blue L dwarfs — the L1 2MASS J13004255+1912354 (hereafter 2MASS J1300+1912; Gizis et al. 2000) the L2 SIPS J0921-2104 (Deacon, Hambly & Cooke 2005), and the L3 2MASS 1721+3344 — to “normal” L dwarfs with

¹⁷ The L subdwarfs 2MASS J05325346+8246465 and 2MASS J16262034+3925190 have considerably larger V_{tan} s consistent with their halo kinematics (Burgasser et al. 2003a; Burgasser 2004).

¹⁸ Obtained through the online database search form created by C. Heise and maintained by P. Smith; see <http://cfa-www.harvard.edu/amdata/ampdata/kurucz23/sekur.html>.

equivalent optical classifications.¹⁹ All four sources are ~ 0.3 – 0.5 mag bluer than the average for their optical spectral type (e.g., Kirkpatrick et al. 2000), and all show enhanced 1.4 μ m H₂O absorption, weak CO absorption and unusually blue spectral energy distributions as compared to their normal L dwarf counterparts.

In addition, there is consistent disagreement between optical and near-infrared classifications amongst these sources. Using the spectral index relations of Reid et al. (2001), we find that near-infrared types are ~ 2 subtypes later than optical types, larger than the uncertainties in these relations; and the near-infrared indices themselves exhibit significant scatter. The similarities between these L dwarfs suggests that their spectral peculiarities have a common origin.

4.2. Why are Blue L Dwarfs Peculiar?

What drives these spectral peculiarities? As noted in § 1, various studies have evoked unresolved multiplicity, subsolar metallicities, high surface gravities and thin condensate clouds as possible causes. We examine each of these possibilities below, focusing primarily on the properties of 2MASS J1126–5003.

4.2.1. Unresolved Multiplicity?

Peculiar spectra commonly arise from the combined light of two blended sources with differing spectral types. Examples include M dwarf plus white dwarf binaries (e.g., Wachter et al. 2003) and L dwarf plus T dwarf binaries (e.g., Cruz et al. 2004; Looper, Kirkpatrick & Burgasser 2007). Folkes et al. (2007) explicitly considered this possibility for 2MASS J1126–5003 in their analysis. Indeed, a case for unresolved multiplicity can be made based on the apparent similarities of this source to the blue L dwarf SDSS J080531.84+481233.0 (hereafter SDSS J0805+4812; Hawley et al. 2002), which itself appears to be a binary (Burgasser 2007b). While Folkes et al. (2007) reject unresolved multiplicity as an explanation for the peculiarity of 2MASS J1126–5003, we examine this possibility again using our more comprehensive spectral coverage.

We compared the near-infrared spectrum of 2MASS J1126–5003 to synthesized binary spectra constructed from SpeX prism data for a large sample of unresolved (i.e., apparently single) L and T dwarfs. Our analysis was identical to that described in Burgasser (2007b), with binary spectra constructed by scaling the spectral templates according to the M_K /spectral type relation of Burgasser (2007a). Figure 6 displays the four best binary fits based on the minimum χ^2 deviation between the normalized spectra.²⁰ The best fitting pair, composed of the L3.5 2MASSW J0036159+182110 (Reid et al. 2000, hereafter 2MASS J0036+1821) and

¹⁹ Additional optical spectral data shown here are from Kirkpatrick et al. (2000); Cruz et al. (2003, 2007) and K. Cruz et al. (in preparation). Additional SpeX prism spectral data shown are from Burgasser et al. (2007); Burgasser (2007b) and K. Cruz et al. (in preparation).

²⁰ Here, $\chi^2 \equiv \sum_{\{\lambda\}} \frac{[f_{\lambda}(D1126) - f_{\lambda}(SB)]^2}{f_{\lambda}(D1126)}$, where $f_{\lambda}(D1126)$ is the spectrum of 2MASS J1126–5003 and $f_{\lambda}(SB)$ the spectrum of the synthesized binary over the set of wavelengths $\{\lambda\} = 1.0$ – 1.35 , 1.45 – 1.8 and 2.0 – 2.35 μ m. See Burgasser (2007b).

the T4 2MASS J21513839-4853542 (Ellis et al. 2005), is a fairly good match in the near-infrared, particularly for the deep H₂O bands and blue spectral energy distribution of 2MASS J1126–5003. However, the weak 1.6 μm CH₄ feature present in the synthesized binary spectrum (also seen in the spectrum of SDSS J0805+4812) is not present in the spectrum of 2MASS J1126–5003. Furthermore, this combination does not reproduce the optical spectrum of 2MASS J1126–5003, as illustrated in Figure 7.²¹ In this case, the T dwarf secondary contributes negligibly to the optical flux of the binary, and as a result the hybrid spectrum is nearly identical to that of 2MASS J0036+1821 (with the notable exception of weaker TiO absorption at 8400 \AA) and inconsistent with that of 2MASS J1126–5003. Binaries with later-type primaries provide a better match at optical wavelengths, but result in stronger CH₄ absorption at 1.6 and 2.2 μm (Figure 6). Similar results were found for alternate L and T dwarf absolute magnitude/spectral type relations (Liu et al. 2006; Burgasser 2007a).

We therefore find no reasonable combination of normal L and T dwarf spectra that can simultaneously reproduce the optical and near-infrared spectrum of 2MASS J1126–5003, confirming the conclusion of Folkes et al. (2007) that this source is likely to be single. It is of course possible that 2MASS J1126–5003 is a binary with peculiar components. However, this scenario is less compelling than that in which 2MASS J1126–5003 is a solitary peculiar L dwarf.

4.2.2. Subsolar Metallicity?

A common explanation for the spectral peculiarities of blue L dwarfs is that their atmospheres are metal-depleted, causing a relative enhancement in collision-induced H₂ absorption that preferentially suppresses flux at *K*-band (Linsky 1969; Saumon et al. 1994; Borysow, Jørgensen, & Zheng 1997). This, along with a general reduction in metal opacity at shorter wavelengths, results in bluer *J* – *K* colors. Indeed, blue near-infrared colors are common for metal-poor M- and L-type subdwarfs (Bessell 1982; Leggett et al. 2000; Burgasser et al. 2003a). Low temperature metal-poor dwarfs also tend to exhibit stronger metal hydride bands and single metal lines due to the greater relative reduction in metal oxide absorption (e.g., Mould & Hyland 1976). This trend is also consistent with enhanced FeH and *J*-band alkali line absorption observed in the near-infrared spectra of 2MASS J1126–5003 (Folkes et al. 2007) and other blue L dwarfs. In addition, L subdwarfs exhibit surprisingly enhanced TiO absorption, unexpected for a metal-depleted atmosphere but consistent with reduced condensate formation (Burgasser et al. 2003a; Gizis & Harvin 2006; Reiners & Basri 2006; Burgasser, Cruz & Kirkpatrick 2007). 2MASS J1126–5003 appears to exhibit this trait as well (Figure 2).

²¹ In this Figure, the spectrum of 2MASS J1126–5003 is compared to a binary template constructed from data for 2MASS J0036+1821 Reid et al. (2000) and the T4.5 2MASS J05591914-1404488 (Burgasser et al. 2000, 2003a), as no optical T4 spectrum was available. The component spectra were scaled to the measured M_{I_c} magnitudes of these sources (16.41 \pm 0.02 and 19.11 \pm 0.07, respectively; Dahn et al. 2002).

However, it is clear that the sources shown in Figure 5 are not as metal-poor as currently known L subdwarfs, given that the latter have far bluer near-infrared colors ($J - K_s \approx 0$) and more peculiar optical and near-infrared spectral morphologies (Gizis & Harvin 2006; Burgasser, Cruz & Kirkpatrick 2007). Furthermore, the Na I, Rb I and Cs I lines in the 7800–8600 \AA spectral band are similar in strength to those of both 2MASS J2224-0158 and 2MASS J1507-1627 (Figure 3), making it unlikely that 2MASS J1126–5003 is significantly metal-poor relative to these sources.

Can the spectral peculiarities seen in blue L dwarf spectra nevertheless be the result of modest subsolar metallicities; e.g., $[M/H] \sim -0.5$? To address this question, we examined trends in the most recent theoretical spectral models from Burrows, Sudarsky & Hubeny (2006). While these models do not as yet reproduce the near-infrared spectra of L dwarfs in detail (cf., Burrows, Sudarsky & Hubeny 2006; Cushing et al. 2007), trends as a function of metallicity can be examined and compared to the deviations observed between normal and blue L dwarfs. Figure 8 illustrates this, comparing two normalized and smoothed condensate cloud models, both assuming $T_{eff} = 1700$ K, $\log g = 5.5$ (cgs) and a modal grain size $a_0 = 100$ μm , but differing in metallicity: $[M/H] = 0$ and -0.5 . Consistent with the arguments above, the lower metallicity model exhibits both a bluer spectral energy distribution and enhanced 0.99 μm FeH absorption, as observed in the blue L dwarfs. However, no enhancement in the 1.4 μm H₂O band is seen, as its opacity is uniformly reduced across most of the near-infrared spectral region. This inconsistency suggests that subsolar metallicity alone cannot explain the spectral peculiarities of blue L dwarfs, even if this is a characteristic trait of such sources.

4.2.3. High Surface Gravity?

Surface gravity influences the emergent spectral energy distribution of a late-type dwarf by modulating the photospheric gas pressure, affecting both pressure-sensitive features and gas/condensate chemistry. Spectral signatures of low surface gravity, including weakened alkali lines, enhanced metal oxide absorption and reduced H₂ absorption (resulting in redder near-infrared colors), have all been used to identify and characterize young brown dwarfs (e.g., Luhman & Rieke 1999; McGovern et al. 2004; Kirkpatrick et al. 2006; Allers et al. 2007). As blue L dwarfs tend to have opposing spectral peculiarities, it is reasonable to consider that these sources may have high surface gravities, a result of being both older and more massive than their equivalently classified counterparts.

As discussed in § 3.4, there is kinematic evidence to support this idea. 2MASS J1126–5003, 2MASS J1300+1921 and 2MASS J1721+3344 all have estimated $V_{tan} \gtrsim 100$ km s^{-1} (Gizis et al. 2000; Cruz et al. 2007), at the 3σ tail of the L dwarf V_{tan} distribution of Schmidt et al. (2007). Knapp et al. (2004) and Cruz et al. (2007) have argued that the large space velocities of blue L dwarfs indicate that they may be members of the old disk or thick disk populations and, as such, are older and more massive than the average field L dwarf. The 2 Gyr lower age limit of 2MASS J1126–5003 based on the absence of Li I absorption in its optical spectrum

is further evidence that this source is relatively old and has a high surface gravity.

However, surface gravity effects alone also fail to explain the spectral peculiarities of 2MASS J1126–5003 and other blue L dwarfs. Figure 9 illustrates trends in surface gravity between $\log g = 5.0$ and 5.5 for the condensate cloud models of Burrows, Sudarsky & Hubeny (2006) and M. Marley et al. (in preparation), assuming $T_{eff} = 1700$ K, solar metallicity, and baseline cloud parameters ($a_0 = 100 \mu\text{m}$ and $f_{sed} = 3$; see Cushing et al. 2007). An increase in surface gravity in the Burrows et al. models results in similar qualitative trends as decreased metallicity, namely bluer near-infrared colors and somewhat stronger FeH and alkali line absorption. However, increasing the surface gravity from $\log g = 5.0$ to 5.5 does not appear to change the depth of the $1.4 \mu\text{m}$ H₂O band in any way. The Marley et al. models do show a change in H₂O band strength with higher surface gravity, but in the opposite sense as observed in the blue L dwarfs; the absorption becomes weaker. The reduction in the H₂O band contrast appears to be due to increased condensate opacity in the higher surface gravity models, affecting the flux peaks but not the deep molecular bands (Ackerman & Marley 2001; Marley et al. 2002). Stronger condensate absorption at J -band counteracts the increased H₂ absorption at K -band, such that $J - K$ colors are only modestly affected by changes in surface gravity in these models (see Figure 8 in Knapp et al. 2004). Hence, while blue L dwarfs like 2MASS J1126–5003 may have higher surface gravities than normal field dwarfs, this trait alone does not explain the spectral peculiarities observed.

4.2.4. Thin Condensate Clouds?

A fourth possibility is that the condensate clouds of blue L dwarfs are somehow thinner or less opaque than those of normal field L dwarfs (Knapp et al. 2004; Chiu et al. 2006; Cruz et al. 2007; Leggett et al. 2007). Reduced condensate opacity in the $1 \mu\text{m}$ spectral region allows other features such as FeH and alkali line absorption to appear stronger at these wavelengths, much as reduced metal oxide absorption allows metal hydride bands and alkali lines to emerge in the red optical spectra of L dwarfs (Kirkpatrick et al. 2000) and late-type M subdwarfs (Burgasser, Cruz & Kirkpatrick 2007). Reduced condensate opacity also increases the contrast between the J -band peak and the base of the $1.4 \mu\text{m}$ H₂O band, producing a deeper feature; and between the J and K -band peaks (the latter dominated by H₂ opacity), resulting in bluer near-infrared colors. Many of the spectral peculiarities observed in blue L dwarfs can be qualitatively explained by a reduction in condensate opacity.

Theoretical spectral models quantitatively confirm these trends as well. Figure 10 compares models from Burrows, Sudarsky & Hubeny (2006) and M. Marley et al. (in preparation) for $T_{eff} = 1700$ K, $\log g = 5.5$ and solar metallicity, but with different treatments for the properties of the condensate cloud layers. For the Burrows et al. models, we compare different values for the condensate modal grain size, $a_0 = 30 \mu\text{m}$ versus $100 \mu\text{m}$. Larger grain sizes for a given total condensate mass corresponds to fewer grains and smaller total opacity (see Figure 6 in Burrows, Sudarsky & Hubeny 2006), resulting in a bluer near-infrared spectral energy

distribution and stronger absorption features at the J -band flux peak. In particular, the $1.4 \mu\text{m}$ H₂O band is clearly enhanced in the larger-grain model. For the Marley et al. models, we compared different values for the f_{sed} parameter, which describes the efficiency of condensate sedimentation. Larger values of f_{sed} correspond to both thinner clouds and larger mean particle sizes (Ackerman & Marley 2001). The trends are qualitatively similar to the Burrows et al. models: stronger atomic and molecular gas features and a bluer near-infrared spectral energy distribution as seen in the blue L dwarfs.

Knapp et al. (2004) have previously demonstrated that the colors of blue L dwarfs can be reproduced with models with thinner clouds (higher values of f_{sed}). Figure 10 demonstrates that the spectra of these sources can be reproduced with thin cloud models as well. The $f_{sed} = 4$, $T_{eff} = 1700$ K and $\log g = 5.5$ model of Marley et al. provides an excellent match to the overall spectral energy distribution of 2MASS J1126–5003, including its blue color and deep FeH and H₂O absorption bands. In contrast, most midtype L dwarf spectra are adequately reproduced assuming $f_{sed} = 2-3$ (Knapp et al. 2004; Cushing et al. 2007, M. Marley et al. in preparation). Cushing et al. (2007) have also found that models with progressively thinner clouds fit progressively bluer objects across the L dwarf/T dwarf transition.

Further evidence that cloud properties play a significant role in the colors of L dwarfs can also be deduced from mid-infrared spectroscopy. Cushing et al. (2006) have recently reported a tentative identification of the Si-O stretching mode in the mid-infrared spectra of three midtype L dwarfs. This feature arises from small silicate grains in the photospheres of cloudy L dwarfs. If differences in the colors of L dwarfs are caused by condensate cloud effects, they should be correlated with the strength of the Si-O feature. This appears to be the case. Figure 12 compares the mid-infrared spectra of two sources from the Cushing et al. (2006) study, the L4.5 2MASS J2224-0158 and the L5 2MASS J1507-1627, whose optical and near-infrared spectra are also shown in Figures 2 and 4. These sources have $J - K_s$ colors that differ by over 0.5 mag, and are $\sim 0.2-0.3$ mag redder and bluer than the average midtype L dwarf, respectively (Kirkpatrick et al. 2000). The $10 \mu\text{m}$ feature noted by Cushing et al. (2006) is clearly weaker in the bluer L dwarf, consistent with the interpretation of thinner and/or larger grained clouds. By analogy, we expect this feature in blue L dwarfs such as 2MASS J1126–5003 to be weaker still. This prediction can be tested with future observations.

The presence of thin (or large-grained) uniform condensate clouds therefore provides an adequate explanation for the spectral peculiarities of 2MASS J1126–5003 and other blue L dwarfs. Folkes et al. (2007) have also proposed a somewhat different interpretation of cloud properties in 2MASS J1126–5003: that the apparently reduced condensate opacity arises from holes in an otherwise thick cloud layer. This draws from an idea set forth by Ackerman & Marley (2001) and Burgasser et al. (2002) to explain the rapid disappearance of cloud opacity across the L dwarf/T dwarf transition. Indeed, Folkes et al. (2007) suggest that 2MASS J1126–5003 is itself an L/T transition object (consistent with its late near-infrared spectral type) that may be “crossing over”

at an early stage, perhaps due to reduced metallicity (see also Burrows, Sudarsky & Hubeny 2006). The mid-type L dwarf optical spectral morphology of this source, much earlier than the optical spectra of any T dwarf observed to date (Burgasser et al. 2003a, J. D. Kirkpatrick et al., in preparation), and the absence of CH₄ absorption at 2.2 μm , a common feature of L9 dwarfs (Geballe et al. 2002), argues against this hypothesis. On the other hand, the blue L dwarf 2MASS J1300+1912 exhibits strong photometric variability (Gelino et al. 2002; Maiti et al. 2005) likely due to cloud structure, including perhaps cloud holes. Monitoring of 2MASS J1126–5003 may provide insight into the “cloud hole” interpretation of this source and blue L dwarfs in general. In any case, the basic premise of Folkes et al. (2007), that 2MASS J1126–5003 has reduced condensate opacity, is in agreement with our analysis.

4.3. Improved Near-Infrared Classification of Blue L Dwarfs

We now readdress the issue of the discrepancies between optical and near-infrared classifications of blue L dwarfs like 2MASS J1126–5003. These arise largely from the enhanced 1.4 μm H₂O band, which as illustrated in Figure 10 is highly sensitive to condensate cloud properties (see also Stephens 2003). Since clouds also influence the near-infrared colors of L dwarfs, one possible way of reconciling these optical and near-infrared types is to use a color-corrected H₂O index, analogous to the color-independent indices used to classify young reddened M and L dwarfs (e.g., Wilking, Greene & Meyer 1999; Allers et al. 2007). We constructed a “hybrid” index:

$$H_2O(c) \approx [H_2O - A]/[H/J] \quad (1)$$

$$\equiv \left[\frac{\int F_{1.33-1.35}}{\int F_{1.58-1.60}} \right], \quad (2)$$

where $H_2O - A$ is defined in Reid et al. (2001) and H/J is defined in Burgasser et al. (2002). Figure 11 compares this ratio with another ratio sampling the 1.4 μm band ($H_2O - H$ from Burgasser et al. 2006a) as a function of optical spectral type (SpT) for a sample of SpeX prism data of unresolved and non-peculiar late-type M and L dwarfs (data from Burgasser 2007a and K. Cruz et al. in preparation) and the five blue L dwarfs shown in Figure 5. Linear fits to the normal M and L dwarfs yield the relations

$$SpT = 47.70 - 43.67[H_2O - H] \quad (3)$$

$$SpT = 27.41 - 16.17[H_2O(c)] \quad (4)$$

with a scatter of 0.9 subtypes for both. The blue L dwarfs clearly stand apart in the spectral type/ $H_2O - H$ comparison, and application of Equation 3 yields near-infrared spectral types that are 3.5-4 subtypes later than their optical types (Table 5). However, the subtypes inferred using Equation 4 for the four blue L dwarfs shown in Figure 5 are consistent with their optical types to within one subtype. Note that SDSS J0805+4812 still stands apart from the locus of spectral type versus $H_2O(c)$, probably because its peculiarities arise from unresolved multiplicity as opposed to cloud effects. We advocate use of

the $H_2O(c)$ ratio, along with ratios sampling the longer wavelength features (e.g., K1 or CH₄-2.2 μm), as cloud-independent estimators for the optical spectral types of single L dwarfs.

As pointed out in § 3.3, there is as yet no formal near-infrared classification scheme for L dwarfs. Existing practice — tying near-infrared indices to optical spectral types — ignores the fact that secondary physical parameters such as the character of condensates and condensate clouds can modify the optical and near-infrared spectra of L dwarfs in different ways. Indeed, blue L dwarfs stand out as peculiar largely because their near-infrared spectra do not conform to the morphologies expected for their optical types. Future efforts at extending the existing L dwarf optical classification scheme to encompass near-infrared spectral morphologies will likely require consideration of additional classification parameters that take into account secondary effects, such as luminosity classes delineate surface gravity effects in stars. (for further discussion of these issues, see Kirkpatrick 2005). The definition of a multi-dimensional near-infrared classification scheme for L dwarfs is clearly beyond the scope of this study. We simply point out that blue L dwarfs such as 2MASS J1126–5003 are likely to serve as useful standards for delineating future “cloud classes” amongst L dwarfs.

5. DISCUSSION

Our analysis in § 4.2 leads us to conclude that the spectral peculiarities of 2MASS J1126–5003 and other blue L dwarfs have their immediate cause in condensate cloud effects, specifically the presence of thin, patchy or large-grained condensate clouds at the photosphere. Subsolar metallicities and high surface gravities in of themselves cannot reproduce the observed spectral peculiarities of these sources. However, it is clear that these latter physical properties must play a role in determining the cloud characteristics of blue L dwarfs. Lower metallicities reduce the metal species available to form condensates, resulting in less condensate material overall. Higher surface gravities may increase the sedimentation rate of condensate grains, potentially resulting in thinner clouds. The large tangential velocities and absence of Li I absorption in the three blue L dwarfs 2MASS J1126–5003, 2MASS J1300+1921 and 2MASS J1721+3344 support the idea that these sources may be relatively old and possibly slightly metal-poor. However, the influence of other physical parameters on condensate cloud properties must also be considered, including rotation rates, vertical upwelling rates (e.g., Saumon et al. 2006) and possibly magnetic field strengths.

An assessment of how these fundamental physical parameters influence the properties of condensate clouds in low-temperature atmospheres is the subject of ongoing theoretical investigations (e.g., Helling et al. 2001; Woitke & Helling 2003; M. Marley, in preparation). Empirical studies are also necessary, particularly those focused on well-characterized samples of blue (and red) L dwarfs. To this end, Table 6 lists all blue L dwarfs currently reported in the literature. We anticipate that this list will grow as near-infrared spectroscopic follow-up of L dwarfs continues.

The authors thank Adam Burrows, Mark Marley and

Didier Saumon for providing spectral models for our analysis and comments on the original manuscript, and Michael Cushing for making available his Spitzer IRS data. We would also like to thank telescope operator Bill Golisch and instrument specialist John Rayner at IRTF, and telescope operator Hernán Nuñez at Magellan for their assistance during the observations. Additional appreciation goes to our anonymous referee for her/his prompt review. This publication makes use of data from the Two Micron All Sky Survey, which is a joint project of the University of Massachusetts and the Infrared Processing and Analysis Center, and funded by the National Aeronautics and Space Administration and the National Science Foundation. 2MASS data were obtained from the NASA/IPAC Infrared Science Archive,

which is operated by the Jet Propulsion Laboratory, California Institute of Technology, under contract with the National Aeronautics and Space Administration. This research has benefitted from the M, L, and T dwarf compendium housed at DwarfArchives.org and maintained by Chris Gelino, Davy Kirkpatrick, and Adam Burgasser. K. L. C is supported by a NSF Astronomy and Astrophysics Postdoctoral Fellowship under AST-0401418. The authors wish to recognize and acknowledge the very significant cultural role and reverence that the summit of Mauna Kea has always had within the indigenous Hawaiian community. We are most fortunate to have the opportunity to conduct observations from this mountain.

Facilities: IRTF(SpeX); Magellan Clay(LDSS-3)

REFERENCES

- Ackerman, A. S., & Marley, M. S. 2001, *ApJ*, 556, 872
 Allard, F., Hauschildt, P. H., Alexander, D. R., Tamanai, A., & Schweitzer, A. 2001, *ApJ*, 556, 357
 Allard, N. F., Allard, F., Hauschildt, P. H., Kielkopf, J. F., & Machin, L. 2003, *A&A*, 411, L473
 Allers, K. N., et al. 2007, *ApJ*, 657, 511
 Allington-Smith, J., et al. 1994, *PASP*, 106, 983
 Bailer-Jones, C. A. L., & Mundt, R. 1999, *A&A*, 348, 800
 —. 2001, *A&A*, 367, 218
 Bessell, M. S. 1982, *PASA*, 4, 417
 Borysow, A., Jørgensen, U. G., & Zheng, C. 1997, *A&A*, 324, 185
 Burgasser, A. J. 2004, *ApJ*, 614, L73
 Burgasser, A. J. 2007a, *ApJ*, 659, 655
 Burgasser, A. J. 2007b, *AJ*, in press
 Burgasser, A. J., Cruz, K. L., & Kirkpatrick, J. D. 2007, *ApJ*, 657, 494
 Burgasser, A. J., Geballe, T. R., Leggett, S. K., Kirkpatrick, J. D., & Golimowski, D. A. 2006a, *ApJ*, 637, 1067
 Burgasser, A. J., Kirkpatrick, J. D., Burrows, A., Liebert, J., Reid, I. N., Gizis, J. E., McGovern, M. R., Prato, L., & McLean, I. S. 2003a, *ApJ*, 592, 1186
 Burgasser, A. J., Kirkpatrick, J. D., Liebert, J., & Burrows, A. 2003a, *ApJ*, 594, 510
 Burgasser, A. J.,Looper, D. L., Kirkpatrick, J. D., & Liu, M. C. 2007, *ApJ*, 658, 557
 Burgasser, A. J., Marley, M. S., Ackerman, A. S., Saumon, D., Lodders, K., Dahn, C. C., Harris, H. C., & Kirkpatrick, J. D. 2002a, *ApJ*, 571, L151
 Burgasser, A. J., McElwain, M. W., Kirkpatrick, J. D., Cruz, K. L., Tinney, C. G., & Reid, I. N. 2004, *AJ*, 127, 2856
 Burgasser, A. J., et al. 2000c, *AJ*, 120, 1100
 Burgasser, A. J., et al. 2002, *ApJ*, 564, 421
 Burrows, A., Marley, M. S., & Sharp, C. M. 2000, *ApJ*, 531, 438
 Burrows, A., & Sharp, C. M. 1999, *ApJ*, 512, 843
 Burrows, A., Sudarsky, D., & Hubeny, I. 2006, *ApJ*, 640, 1063
 Burrows, A., & Volobuyev, M. 2003, *ApJ*, 583, 985
 Burrows, A., et al. 1997, *ApJ*, 491, 856
 Cannon, R. D. 1984, in *Astronomy with Schmidt-Type Telescopes*, Proc. IAU Coll. 78, ed. M. Cappaccioli (Dordrecht: Reidel), p. 25
 Chabrier, G., Baraffe, I., Allard, F., & Hauschildt, P. 2000, *ApJ*, 542, 464
 Chiu, K., Fan, X., Leggett, S. K., Golimowski, D. A., Zheng, W., Geballe, T. R., Schneider, D. P., & Brinkmann, J. 2006, *ApJ*, in press
 Cohen, M., Wheaton, W. A., & Megeath, S. T. 2003, *AJ*, 126, 1090
 Cooper, C. S., Sudarsky, D., Milson, J. A., Lunine, J. I., & Burrows, A. 2003, *ApJ*, 586, 1320
 Cruz, K. L., Burgasser, A. J., Reid, I. N., & Liebert, J. *ApJ*, 2004, 604, L61
 Cruz, K. L., Reid, I. N., Liebert, J., Kirkpatrick, J. D., & Lowrance, P. J. 2003, *AJ*, 126, 2421
 Cruz, K. L., et al. 2007, *AJ*, 133, 439
 Cushing, M. C., Vacca, W. D., & Rayner, J. T. 2004, *PASP*, 116, 362
 Cushing, M. C., et al. 2006, *ApJ*, in press
 Cushing, M. C., et al. 2007, *ApJ*, submitted
 Dahn, C. C., et al. 2002, *AJ*, 124, 1170
 Deacon, N. R., Hambly, N. C., & Cooke, J. A. 2005, *A&A*, 435, 363
 Dehnen, W., & Binney, J. J. 1998, *MNRAS*, 298, 387
 Delfosse, X., et al. 1997, *A&A*, 327, L25
 Ellis, S. C., Tinney, C. G., Burgasser, A. J., Kirkpatrick, J. D., & McElwain, M. W. 2005, *AJ*, 130, 2347
 Epchtein, N., et al. 1997, *The Messenger*, 87, 27
 Fegley, B., & Lodders, K. 1996, *ApJ*, 472, L37
 Folkers, S. L., Pinfield, D. J., Kendall, T. R., & Jones, H. R. A. 2007, *MNRAS*, 378, 901
 Geballe, T. R., et al. 2002, *ApJ*, 564, 466
 Gelino, C. R., Marley, M. S., Holtzman, J. A., Ackerman, A. S., & Lodders, K. 2002, *ApJ*, 577, 433
 Gizis, J. E., & Harvin, J. 2006, *AJ*, 132, 2372
 Gizis, J. E., Monet, D. G., Reid, I. N., Kirkpatrick, J. D., Liebert, J., & Williams, R. 2000, *AJ*, 120, 1085
 Golimowski, D. A., et al. 2004, *AJ*, 127, 3516
 Hambly, N. C., Davenhall, A. C., Irwin, M. J., & MacGillivray, H. T. 2001a, *MNRAS* 326, 1315
 Hambly, N. C., Irwin, M. J., & MacGillivray, H. T. 2001b, *MNRAS* 326, 1295
 Hambly, N. C., MacGillivray, H. T., Read, M. A., et al. 2001c, *MNRAS* 326, 1279
 Hamuy, M., Suntzeff, N. B., Heathcote, S. R., Walker, A. R., Gigoux, P., & Phillips, M. M. 1994, *PASP*, 106, 566
 Hartley, M., & Dawe, J. A. 1981, *PASA*, 4, 251
 Hawley, S. L., Gizis, J. E., & Reid, I. N. 1996, *AJ*, 112, 2799
 Hawley, S. L., et al. 2002, *AJ*, 123, 3409
 Helling, C., Oevermann, M., Lüttke, M. J. H., Klein, R., & Sedlmayr, E. 2001, *A&A*, 376, 194
 Houck, J. R., et al. 2004, *ApJS*, 154, 18
 Jones, H. R. A., & Tsuji, T. 1997, *ApJ*, 480, L39
 Kirkpatrick, J. D. 2005, *ARA&A*, 43, 195
 Kirkpatrick, J. D., Barman, T. S., Burgasser, A. J., McGovern, M. R., McLean, I. S., Tinney, C. G., & Lowrance, P. J. 2006, *ApJ*, 639, 1120
 Kirkpatrick, J. D., Reid, I. N., Liebert, J., Gizis, J. E., Burgasser, A. J., Monet, D. G., Dahn, C. C., Nelson, B., & Williams, R. J. 2000, *AJ*, 120, 447
 Kirkpatrick, J. D., et al. 1999, *ApJ*, 519, 802
 Knapp, G., et al. 2004, *ApJ*, 127, 3553
 Kurucz, R. L., & Bell, B. 1995, *Atomic Line Data*, Kurucz CD-ROM No. 23. (Cambridge: Smithsonian Astrophysical Observatory)
 Leggett, S. K., Allard, F., Dahn, C., Hauschildt, P. H., Kerr, T. H., & Rayner, J. 2000, *ApJ*, 535, 965
 Leggett, S. K., Saumon, D., Marley, M. S., Geballe, T. R., Golimowski, D. A., Stephens, D., & Fan, X. *ApJ*, 655, 1079
 Lépine, S., Rich, R. M., & Shara, M. M. 2003, *ApJ*, 591, L49
 Linsky, J. L. 1969, *ApJ*, 156, 989
 Liu, M. C., Leggett, S. K., Golimowski, D. A., Chiu, K., Fan, X., Geballe, T. R., Schneider, D. P., & Brinkmann, J. 2006, *ApJ*, 647, 1393

- Lodders, K. 2002, *ApJ*, 577, 974
- Looper, D. L., Kirkpatrick, J. D., & Burgasser, A. J., *AJ*, 134, 1162
- Luhman, K. L., & Rieke, G. H. 1999, *ApJ*, 525, 440
- Maiti, M., Sengupta, S., Parihar, P. S., & Anupama, G. C. 2005, *ApJ*, 619, L183
- Marley, M. S., Saumon, D., Guillot, T., Freedman, R. S., Hubbard, W. B., Burrows, A., & Lunine, J. I. 1996, *Science*, 272, 1919
- Marley, M. S., Seager, S., Saumon, D., Lodders, K., Ackerman, A. S., Freedman, R., & Fan, X. 2002, *ApJ*, 568, 335
- Martín, E. L., Delfosse, X., Basri, G., Goldman, B., Forveille, T., & Zapatero Osorio, M. R. 1999, *AJ*, 118, 2466
- McElwain, M. W., & Burgasser, A. J. 2006, *AJ*, in press
- McGovern, M. R., Kirkpatrick, J. D., McLean, I. S., Burgasser, A. J., Prato, L., & Lowrance, P. J. 2004, *ApJ*, 600, 1020
- McLean, I. S., McGovern, M. R., Burgasser, A. J., Kirkpatrick, J. D., Prato, L., & Kim, S. 2003, *ApJ*, 596, 561
- Mohanty, S., & Basri, G. 2003, *ApJ*, 583, 451
- Mohanty, S., Basri, G., Shu, F., Allard, F., & Chabrier, G. 2002, *ApJ*, 572, 469
- Mould, J. R., & Hyland, A. R. 1976, *ApJ*, 208, 399
- Oke, J. B., et al. 1995, *PASP*, 107, 375
- Rayner, J. T., Toomey, D. W., Onaka, P. M., Denault, A. J., Stahlberger, W. E., Vacca, W. D., Cushing, M. C., & Wang, S. 2003, *PASP*, 155, 362
- Rebolo, R., Martín, E. L., & Magazzu, A. 1992, *ApJ*, 389, L83
- Reid, I. N., Burgasser, A. J., Cruz, K., Kirkpatrick, J. D., & Gizis, J. E. 2001, *AJ*, 121, 1710
- Reid, I. N., Kirkpatrick, J. D., Gizis, J. E., Dahn, C. C., Monet, D. G., Williams, R. J., Liebert, J., & Burgasser, A. J. 2000, *AJ*, 119, 369
- Reiners, A., & Basri, G. 2006, *AJ*, 131, 1806
- Saumon, D., Bergeron, P., Lunine, J. I., Hubbard, W. B., & Burrows, A. 1994, *ApJ*, 424, 333
- Saumon, D., et al. 2006, *ApJ*, 656, 1136
- Schmidt, S. J., Cruz, K. L., Bongiorno, B. J., Liebert, J., & Reid, I. N. 2007, *AJ*, in press
- Skrutskie, M. F., et al. 2006, *AJ*, 131, 1163
- Stephens, D. C. 2003, in *IAU Symposium 211, Brown Dwarfs*, ed. E. Martín (San Francisco: ASP), p. 355
- Tinney, C. G., Burgasser, A. J., & Kirkpatrick, J. D. 2003, *AJ*, 126, 975
- Tokunaga, A. T., & Kobayashi, N. 1999, *AJ*, 117, 1010
- Tsuji, T. 2005, *ApJ*, 621, 1033
- Tsuji, T., Ohnaka, K., & Aoki, W. 1996, *A&A*, 305, L1
- Tsuji, T., Ohnaka, K., Aoki, W., & Nakajima, T. 1996, *A&A*, 308, L29
- Vacca, W. D., Cushing, M. C., & Rayner, J. T. 2003, *PASP*, 155, 389
- Vrba, F. J., et al. 2004, *AJ*, 127, 2948
- Wachter, S., Hoard, D. W., Hansen, K. H., Wilcox, R. E., Taylor, H. M., & Finkelstein, S. L. 2003, *ApJ*, 586, 1356
- West, A. A., et al. 2004, *AJ*, 128, 426
- Wilking, B. A., Greene, T. P., & Meyer, M. R. 1999, *AJ*, 117, 469
- Woitke & Helling, C. 2003, *A&A*, 399, 297

TABLE 1
ASTROMETRY FOR 2MASS J11263991–5003550.

α^a	δ^a	Epoch	Catalog
11 ^h 26 ^m 42 ^s .65	-50°04′02″.4	13 Jan 1983	ESO; SSS
11 ^h 26 ^m 42 ^s .24	-50°04′01″.4	13 Mar 1985	UKST; SSS
11 ^h 26 ^m 39 ^s .93	-50°03′55″.3	06 Apr 1999	DENIS
11 ^h 26 ^m 39 ^s .91	-50°03′55″.0	10 May 1999	2MASS
11 ^h 26 ^m 39 ^s .89	-50°03′55″.3	30 May 1999	DENIS

^a Equinox J2000 coordinates.

TABLE 2
EQUIVALENT WIDTHS OF
OPTICAL LINES.

Line	EW (Å)
H α (6563 Å)	> -0.5 ^a
Li I (6708 Å)	< 0.4 ^a
Rb I (7800 Å)	5.6±0.3
Rb I (7948 Å)	5.6±0.3
Na I (8183/8195 Å)	5.6±0.2
Cs I (8521 Å)	3.5±0.2

^a 1 σ upper/lower limits.

TABLE 3
SPECTRAL INDICES AND CLASSIFICATION.

Index	Optical			Near-infrared			
	Value	Subtype ^a	Ref	Index	Value	Subtype ^a	Ref
CrH-a	1.79	L3.5	1	H ₂ O-A	0.46	L8.5	4
Rb-b/TiO-b	1.59	L4.5	1	H ₂ O-B	0.57	L6.5	4
Cs-a/VO-b	1.33	L4.5	1	K1	0.34	L4.5	4,5
Color-d	11.87	L5	1	H ₂ O 1.5 μ m	1.74	[L8]	6
K I fit	...	L5	1	CH ₄ 2.2 μ m	1.02	[L5.5]	6
PC3	6.58	[L5] ^b	2	H ₂ O-J	0.74	[L6]	7,8
VO7434	1.62	[L6]	3	H ₂ O-H	0.65	[L8]	7,8
Na8190	1.05	[L3]	3	CH ₄ -K	0.98	[L5]	7,8
TiO8440	0.82	[L3]	3	H ₂ O	1.47	[L7.5]	9
				H ₂ O(c)	0.72	[L5.5]	10
Optical Type	L4.5±0.5			NIR Type	L6.5±2 (pec)		

REFERENCES. — (1) Kirkpatrick et al. (1999); (2) Martín et al. (1999); (3) Hawley et al. (2002); (4) Reid et al. (2001); (5) Tokunaga & Kobayashi (1999); (6) Geballe et al. (2002); (7) Burgasser et al. (2006a); (8) Burgasser (2007a); (9) Allers et al. (2007); (10) This paper.

^a Subtypes in brackets were not used to compute the final average type.

^b Consistent with measurements for DENIS J1228-1547 (Delfosse et al. 1997; Martín et al. 1999), classified L5 on the Kirkpatrick et al. (1999) scheme.

TABLE 4
 PROPERTIES OF 2MASS J11263991–5003550.

Parameter	Value	Reference
α^a	11 ^h 26 ^m 39 ^s .91	1
δ^a	–50° 03′ 55″.0	1
μ	1″.66±0″.03 yr ^{–1}	1,2,3
θ	285° 3±1° 6	1,2,3
Optical SpT	L4.5	3
NIR SpT	L6.5±2 (pec)	3
Distance ^{b,c}	15±2 pc	3
V_{tan}^b	117±15 km s ^{–1}	3
V_{rad}	46±9 km s ^{–1}	3
$(U, V, W)^b$	(85, –98, –6) km s ^{–1}	3
T_{eff}^b	≈1700 K	4,5
Mass ^{b,d}	>0.065 M _⊙	3
Age ^{b,d}	>2 Gyr	3,6
R_{ESO}	20.36 mag	2
I_N	17.60 mag	2
I	17.80±0.15 mag	7
J	14.00±0.03 mag	1
H	13.28±0.04 mag	1
K_s	12.83±0.03 mag	1
$I - J$	3.80±0.15 mag	1,7
$J - H$	0.72±0.05 mag	1
$H - K_s$	0.45±0.05 mag	1
$J - K_s$	1.17±0.04 mag	1

REFERENCES. — (1) 2MASS (Skrutskie et al. 2006); (2) SSS (Hambly et al. 2001a,b,c); (3) This paper; (4) Golimowski et al. (2004); (5) Vrba et al. (2004); (6) Burrows et al. (1997); (7) DENIS (Epchtein et al. 1997).

^a Equinox J2000 coordinates at epoch 10 May 1999 from 2MASS.

^b Estimated; see § 3.4.

^c Assuming this source is single; see § 4.2.1.

^d Based on the absence of Li I absorption at 6708 Å; see § 3.1.

TABLE 5
 NEAR-INFRARED CLASSIFICATIONS OF BLUE L DWARFS IN FIGURE 5.

Source	Optical SpT	H ₂ O-A ^a	H ₂ O-B ^a	K1 ^a	H ₂ O-H ^b	H ₂ O(c) ^{b,c}	NIR SpT ^d
2MASSW J1300425+191235	L1	0.62 (L3.5)	0.69 (L3.5)	0.24 (L2.5)	0.76 (L4.5)	1.04 (L0.5)	L3±0.5
SIPS J0921-2104	L2	0.56 (L5.5)	0.67 (L4)	0.25 (L2.5)	0.74 (L5.5)	0.95 (L2)	L4±1.5
2MASS J1721039+334415	L3	0.54 (L6)	0.62 (L5.5)	0.30 (L4)	0.71 (L7)	0.90 (L3)	L5±1
2MASS J11263991–5003550	L4.5	0.46 (L8.5)	0.57 (L6.5)	0.34 (L4.5)	0.65 (L9)	0.72 (L5.5)	L6.5±2

^a Indices and index/spectral type relations from Reid et al. (2001).

^b Indices and index/spectral type relations from Burgasser et al. (2002) and this paper (Eqn. 3 and 4).

^c Color-corrected H₂O index.

^d Based only on the Reid et al. (2001) indices.

TABLE 6
BLUE L DWARFS REPORTED IN THE LITERATURE.

Source	Spectral Type Optical/NIR	V_{tan} (km s ⁻¹)	J (mag)	$J - K_s$ (mag)	$\Delta(J - K_s)^a$ (mag)	Ref.
SDSS J080531.84+481233.0 ^b	L4/L9.5:	...	14.73±0.04	1.29±0.05	-0.58	1,2,3,4,5
SIPS J0921-2104	L2/L4: ^c	58	12.78±0.02	1.09±0.03	-0.62	6,7,8,9
SDSS J093109.56+032732.5	-/L7.5:	...	16.62±0.14	<0.88	...	2
SDSS J103321.92+400549.5	-/L6	...	16.64±0.16	<1.24	...	3
SDSS J112118.57+433246.5	-/L7.5	...	17.01±0.20	1.49±0.29	...	3
2MASS J11263991–5003550	L4.5/L6.5: ^c	117	14.00±0.03	1.17±0.04	-0.82	8,10
SDSS J142227.25+221557.1	-/L6.5:	...	17.06±0.18	1.42±0.25	...	3
2MASSW J1300425+191235	L1/L3.5 ^c	98	12.72±0.02	1.09±0.03	-0.33	9,11,12,13
SDSS J133148.92-011651.4	L6/L8:	...	15.46±0.04	1.39±0.08	-0.34	1,2
2MASSI J1721039+334415	L3/L5: ^c	139	13.63±0.02	1.14±0.03	-0.58	9,12,13

REFERENCES. — (1) Hawley et al. (2002); (2) Knapp et al. (2004); (3) Chiu et al. (2006); (4) Burgasser (2007b); (5) J. D. Kirkpatrick et al. (in preparation); (6) Deacon, Hambly & Cooke (2005); (7) I. N. Reid et al. (in preparation); (8) This paper; (9) Schmidt et al. (2007); (10) Folkes et al. (2007); (11) Gizis et al. (2000); (12) Cruz et al. (2003); (13) Cruz et al. (2007)

^a Difference in $J - K_s$ color from the average of L dwarfs with similar optical spectral type (Kirkpatrick et al. 2000).

^b This source appears to be an unresolved binary system (Burgasser 2007b).

^c See Table 5.

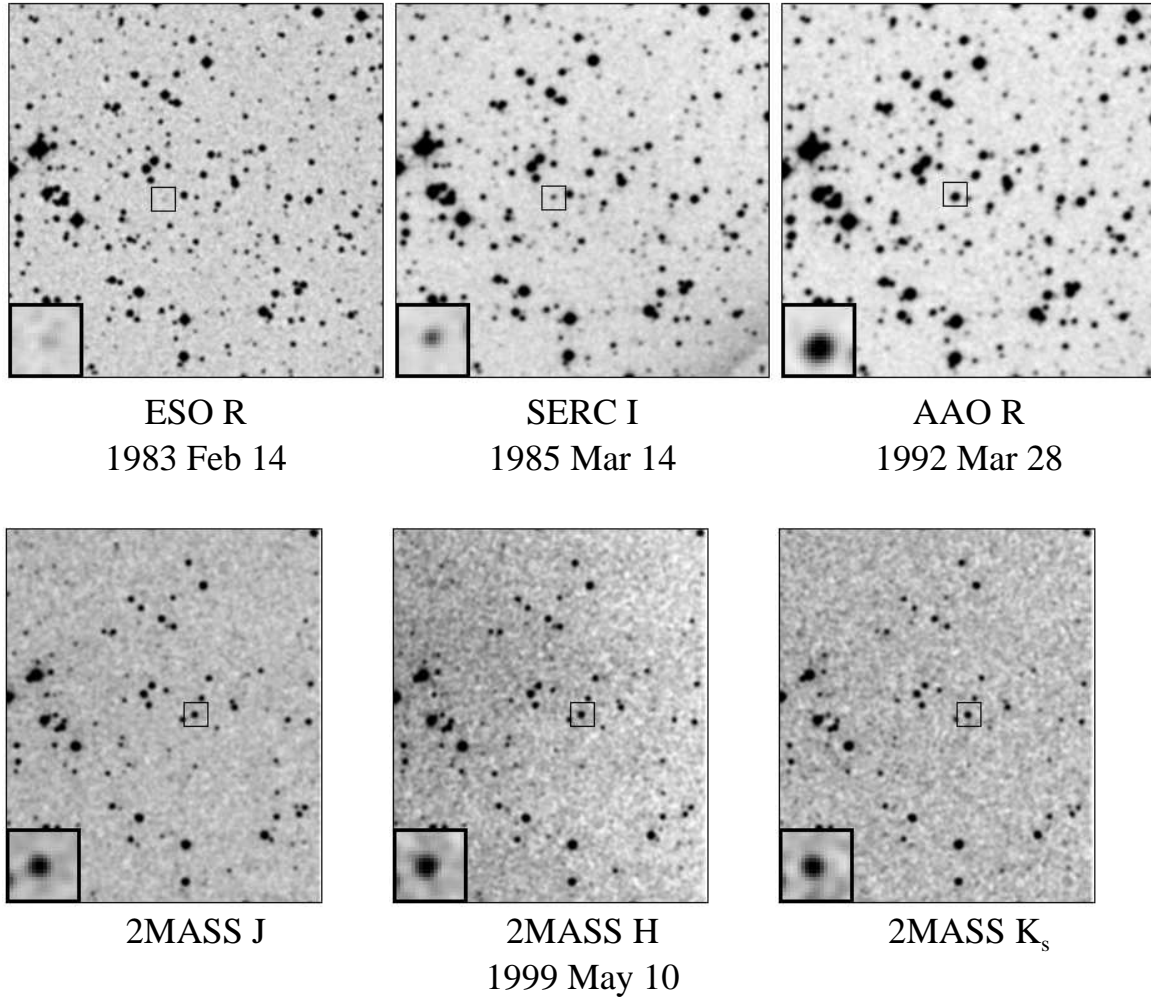


FIG. 1.— Field images of 2MASS J11263991–5003550 from ESO R (top left), SERC I_N (top middle) and AAO R (top right) photographic plates; and 2MASS JHK_s (bottom). All images are scaled to the same spatial resolution and oriented with north up and east to the left. Photographic plate images are $5'$ on a side. Inset boxes $20'' \times 20''$ in size in each image indicate the position of the source after correcting for its motion ($\mu = 1''.66 \pm 0''.03 \text{ yr}^{-1}$ at position angle $\theta = 285^\circ.3 \pm 1^\circ.6$) and are expanded in the lower left corner. Note that the bright optical source close to the motion-corrected position of 2MASS J1126–5003 in the 1992 AAO R image is a background star.

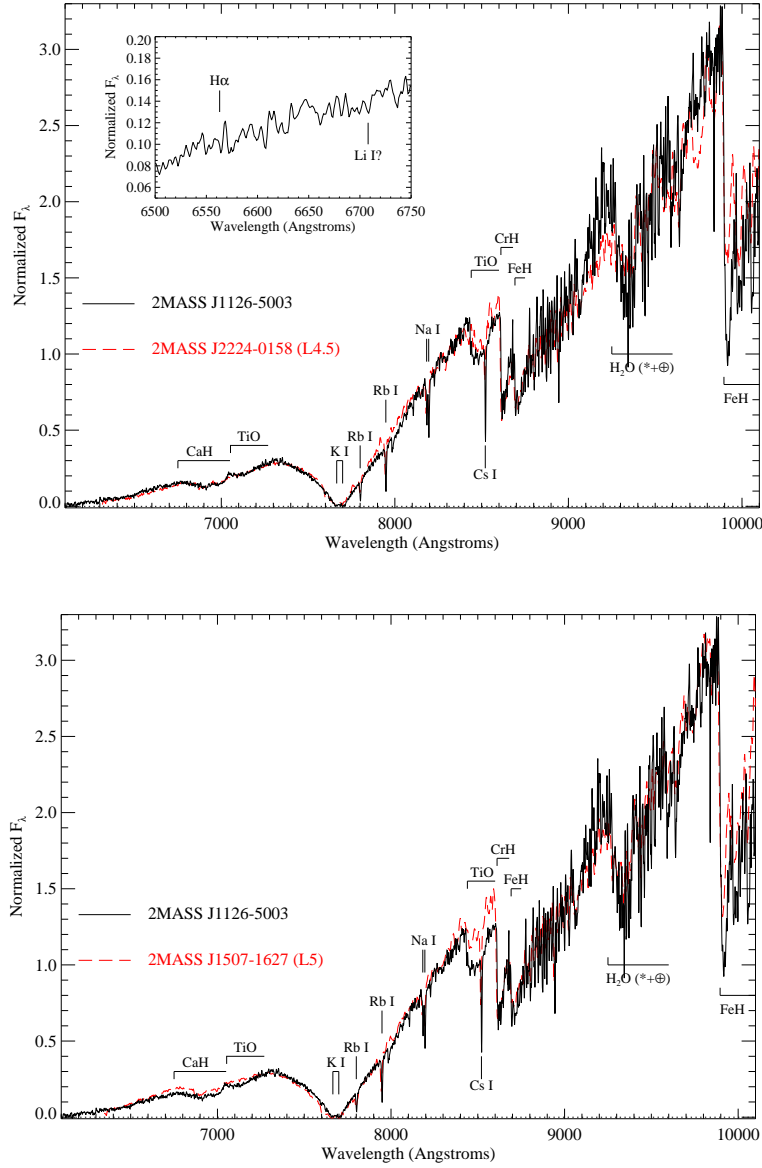


FIG. 2.— Red optical (6100–10100 Å) spectrum of 2MASS J1126–5003 (black lines) obtained with LDSS-3, compared to the LRIS spectra of the L4.5 2MASS J2224-0158 (top panel, red dashed line) and the L5 2MASS J1507-1627 (bottom panel, red dashed line) from Kirkpatrick et al. (2000). All spectra are normalized at 8200 Å. Note that the spectrum of 2MASS J1126–5003 has been corrected for telluric absorption shortward of 9000 Å, while those of 2MASS J2224-0158 and 2MASS J1507-1627 have not. Major molecular and atomic absorption features are labelled. The inset box in the top panel expands the 6500–6750 Å spectrum of 2MASS J1126–5003 hosting the 6563 Å $H\alpha$ emission and 6708 Å Li I absorption lines, neither of which are convincingly detected.

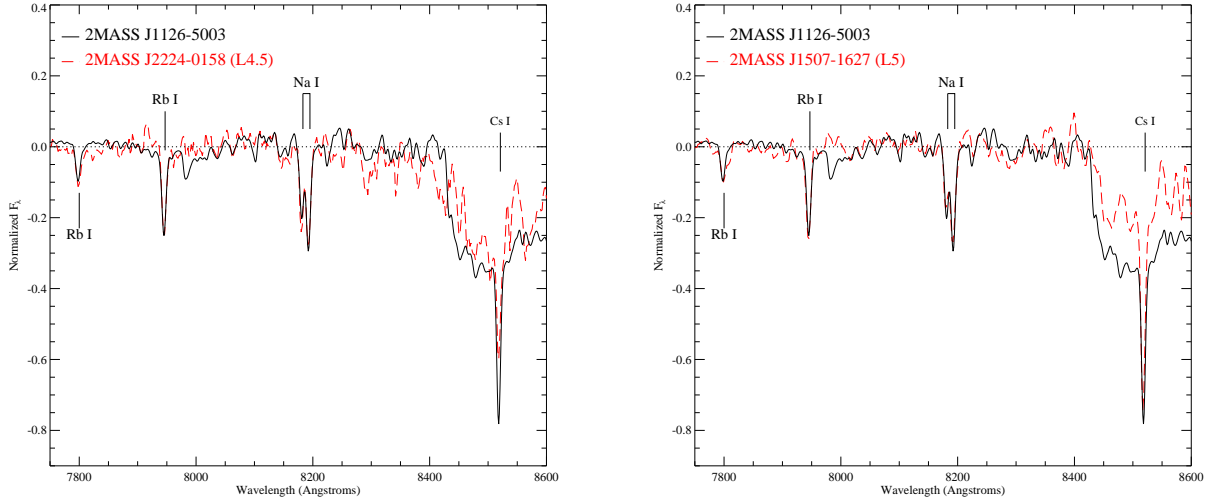


FIG. 3.— Red optical alkali lines (Rb I, Na I and Cs I) in the 7750–8300 Å spectral region of 2MASS J1126–5003 (black lines) compared to the L4.5 2MASS J2224-0158 (left panel, red dashed line) and the L5 2MASS J1507-1627 (right panel, red dashed line). A linear fit to the local continuum in this spectral range has been subtracted from all spectra to highlight the line absorption, and data have been deconvolved to the same resolution ($\lambda/\Delta\lambda = 1000$) and shifted to their frame of rest for accurate comparison.

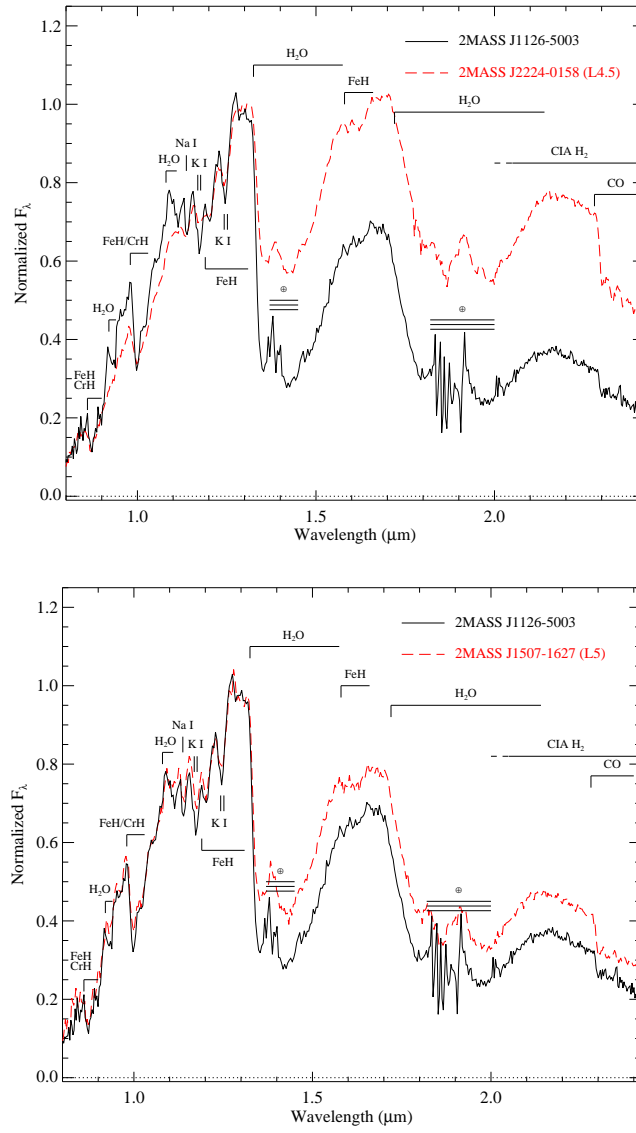


FIG. 4.— Near-infrared SpeX prism spectra of 2MASS J1126–5003 (black line) compared to the L4.5 2MASS J2224-0158 (top panel, red dashed line), and the L5 2MASS J1507-1627 (bottom panel, red dashed line). All spectra are normalized at $1.28 \mu\text{m}$. Major molecular (FeH, CrH, H₂O, CO, H₂) and atomic (Na I and K I) absorption features are labelled, as well as regions of strong telluric absorption (\oplus).

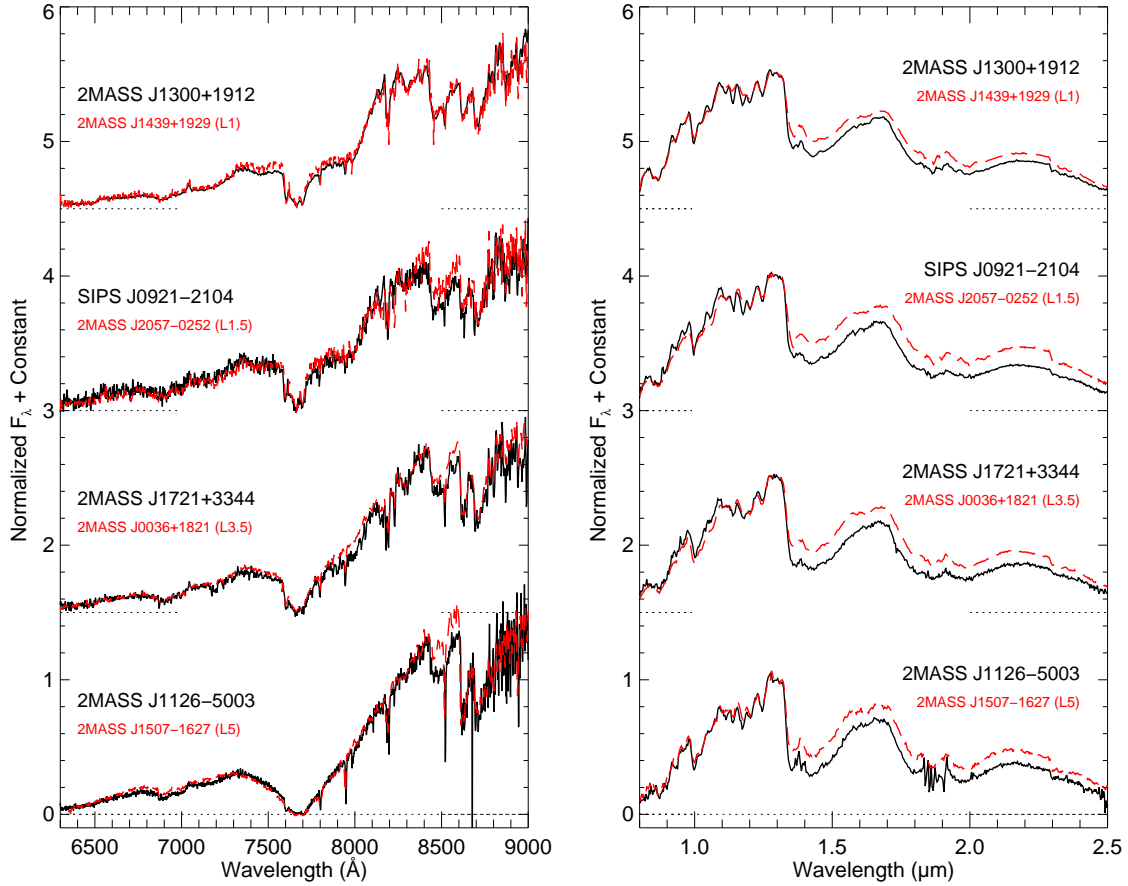


FIG. 5.— Comparison of optical (left panel, 6300–9000 Å) and near-infrared (right panel, 0.9–2.4 μm) spectra of the four blue L dwarfs 2MASS J1300+1912, SIPS J0921-2104, 2MASS J1721+3344 and 2MASS J1126–5003 (black lines, from top to bottom). These are compared to field L dwarf spectral templates 2MASS 14392836+1929149 (L1; Kirkpatrick et al. 1999), 2MASS J20575409-0252302 (L1.5; Cruz et al. 2003), 2MASS J00361617+1821104 (L3.5; Reid et al. 2000) and 2MASS J1507-1627 (L5; Reid et al. 2000; red dashed lines). All spectra are normalized at 8200 Å (left panel) or 1.28 μm (right panel) and offset by constants (dotted lines). Note that the blue L dwarfs show reasonable agreement with their spectral comparison sources up to the $\sim 1.3 \mu\text{m}$ H_2O band, but are depressed (to varying degrees) at longer wavelengths.

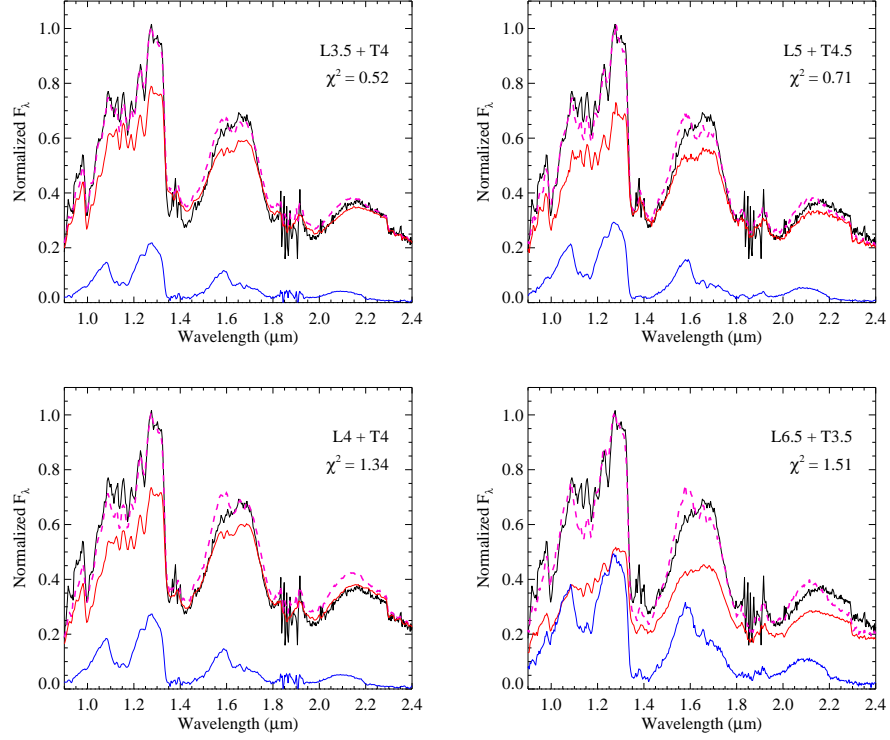


FIG. 6.— Best-fitting binary brown dwarf templates to the near-infrared spectrum of 2MASS J1126–5003. Data for the source (black lines) and spectra of the binary composites (purple dashed lines) are normalized at $1.27 \mu\text{m}$. Primary (red solid lines) and secondary (blue solid lines) template spectra are scaled to their relative contributions to the composite spectra. The spectral types of the components (optical for L dwarfs, near-infrared for T dwarfs) are indicated in the upper right corner of each panel, along with χ^2 deviations.

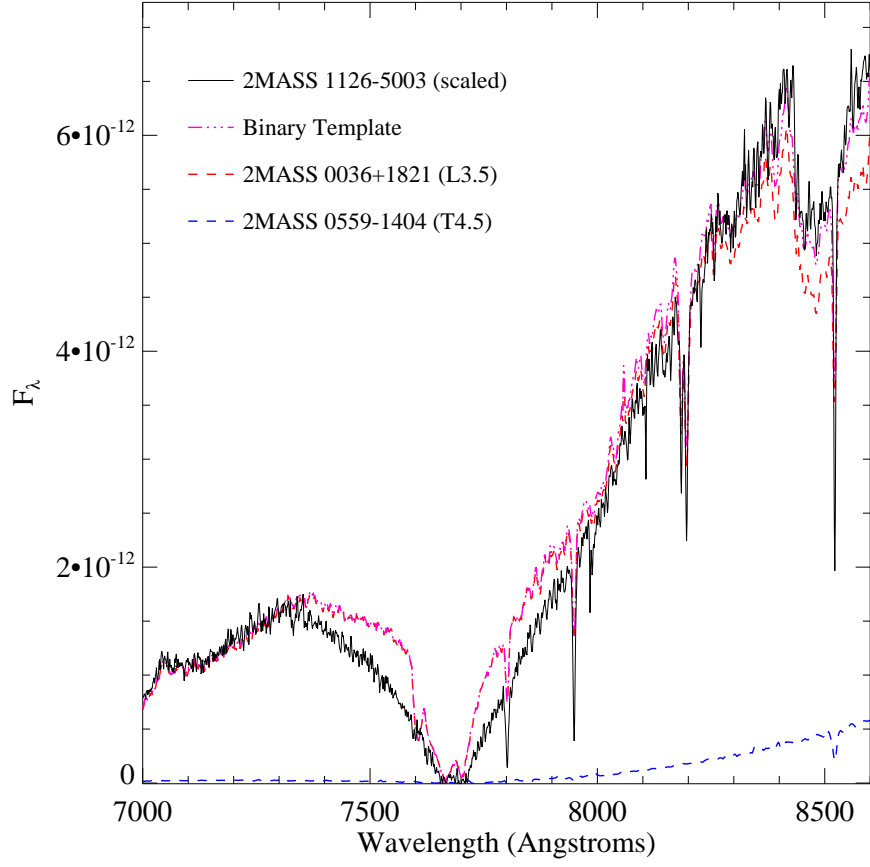


FIG. 7.— Comparison of a composite binary spectrum (purple dashed line) composed of L3.5 2MASS J0036+1821 (red triple-dot-dashed line) and T4.5 2MASS J0559-1404 (blue triple-dot-dashed line) template spectra, to optical data for 2MASS J1126–5003 (black solid line). The templates are scaled to their M_{I_c} magnitudes as measured by Dahn et al. (2002), and the spectrum of 2MASS J1126–5003 is scaled to provide a best fit to the composite spectrum.

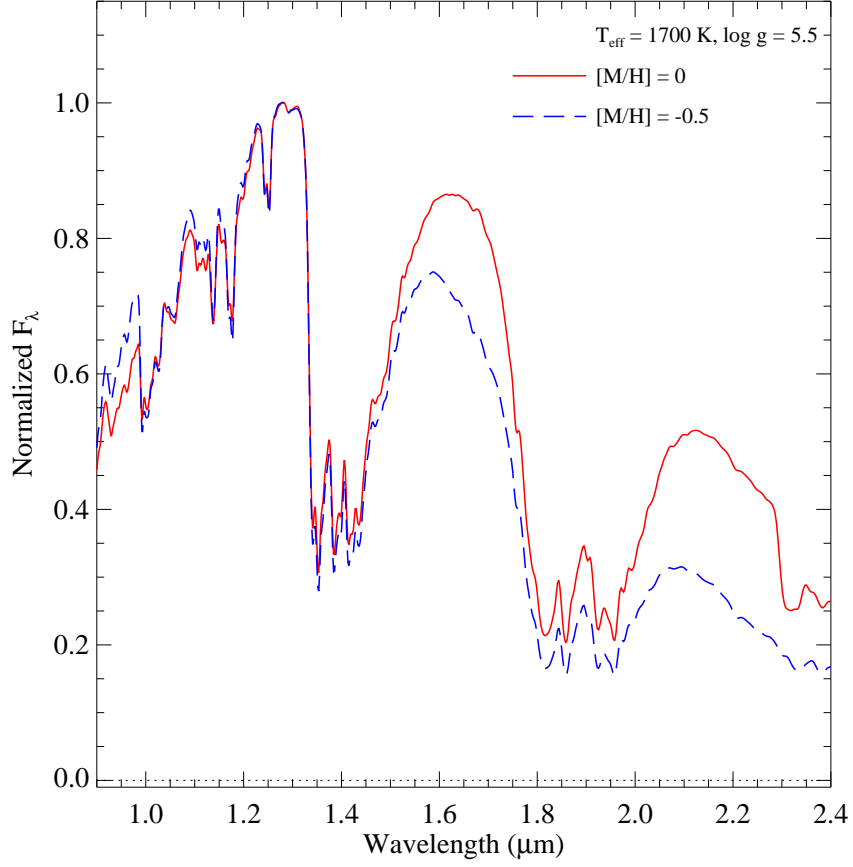


FIG. 8.— Comparison of metallicity effects in the spectral models of Burrows, Sudarsky & Hubeny (2006). Both models shown assume $T_{\text{eff}} = 1700 \text{ K}$, $\log g = 5.5$ (cgs) and a modal condensate particle size $a_0 = 100 \mu\text{m}$, but differ in metallicity (red solid line: $[M/H] = 0$, blue dashed line: $[M/H] = -0.5$). The model spectra have been smoothed to a resolution of $\lambda/\Delta\lambda = 120$ using a Gaussian kernel, similar to that of the SpeX data, and are normalized at $1.27 \mu\text{m}$.

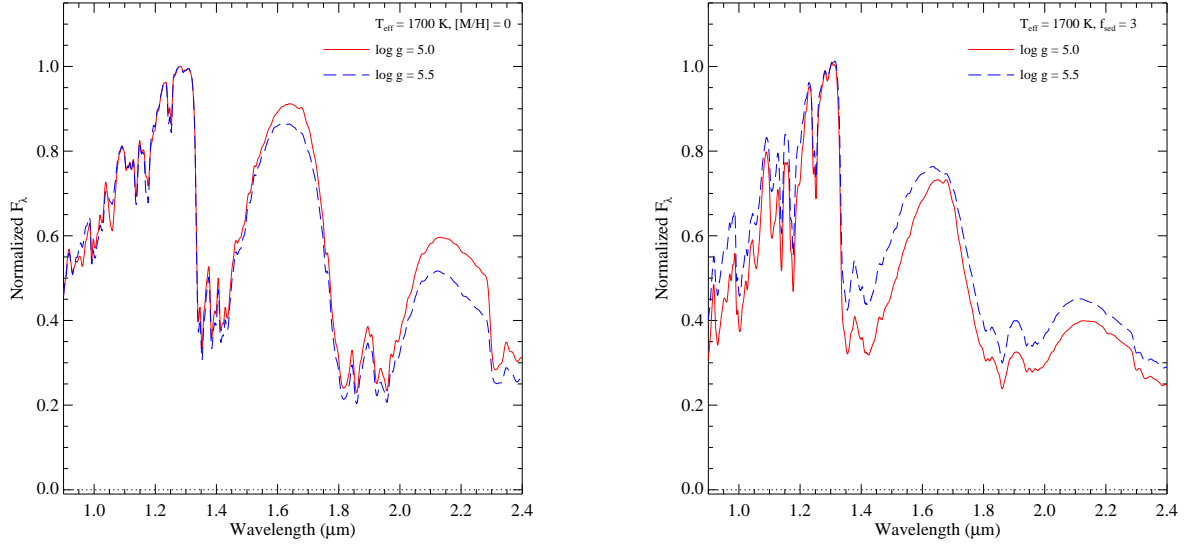


FIG. 9.— Comparison of gravity effects in the spectral models of Burrows, Sudarsky & Hubeny (2006, left) and M. Marley et al. (in preparation; right). All models assume $T_{eff} = 1700$ K and solar metallicity but differ in surface gravity (red solid lines: $\log g = 5.0$, blue dashed lines: $\log g = 5.5$). All model spectra have been smoothed to a resolution of $\lambda/\Delta\lambda = 120$ using a Gaussian kernel and are normalized at $1.27 \mu\text{m}$.

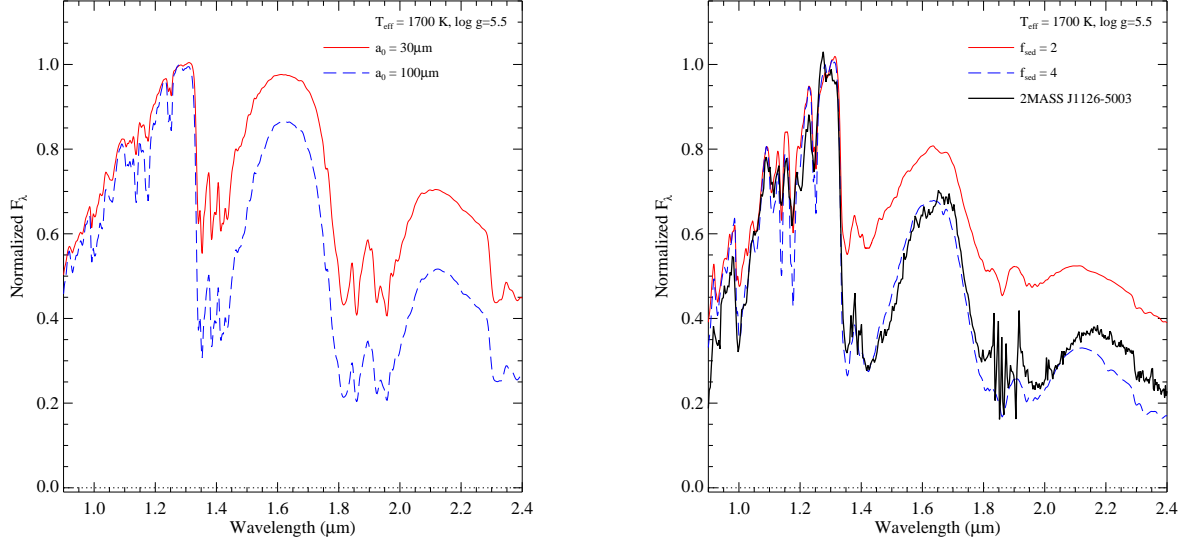


FIG. 10.— Comparison of condensate cloud effects in the spectral models of Burrows, Sudarsky & Hubeny (2006, left) and M. Marley et al. (in preparation; right). All models assume $T_{\text{eff}} = 1700 \text{ K}$, solar metallicity, and $\log g = 5.5$. The Burrows et al. models differ in their modal condensate particle size, with $a_0 = 30 \mu\text{m}$ (red solid line) and $100 \mu\text{m}$ (blue dashed line) shown. The Marley et al. models differ in the assumed sedimentation efficiency, with $f_{\text{sed}} = 2$ (red solid line) and 4 (blue dashed line) shown. Also shown in the right panel is the spectrum of 2MASS J1126–5003 (black solid line), which shows adequate agreement with the $f_{\text{sed}} = 4$ model of Marley et al. Model spectra have been smoothed to a resolution of $\lambda/\Delta\lambda = 120$ using a Gaussian kernel and are normalized at $1.27 \mu\text{m}$.

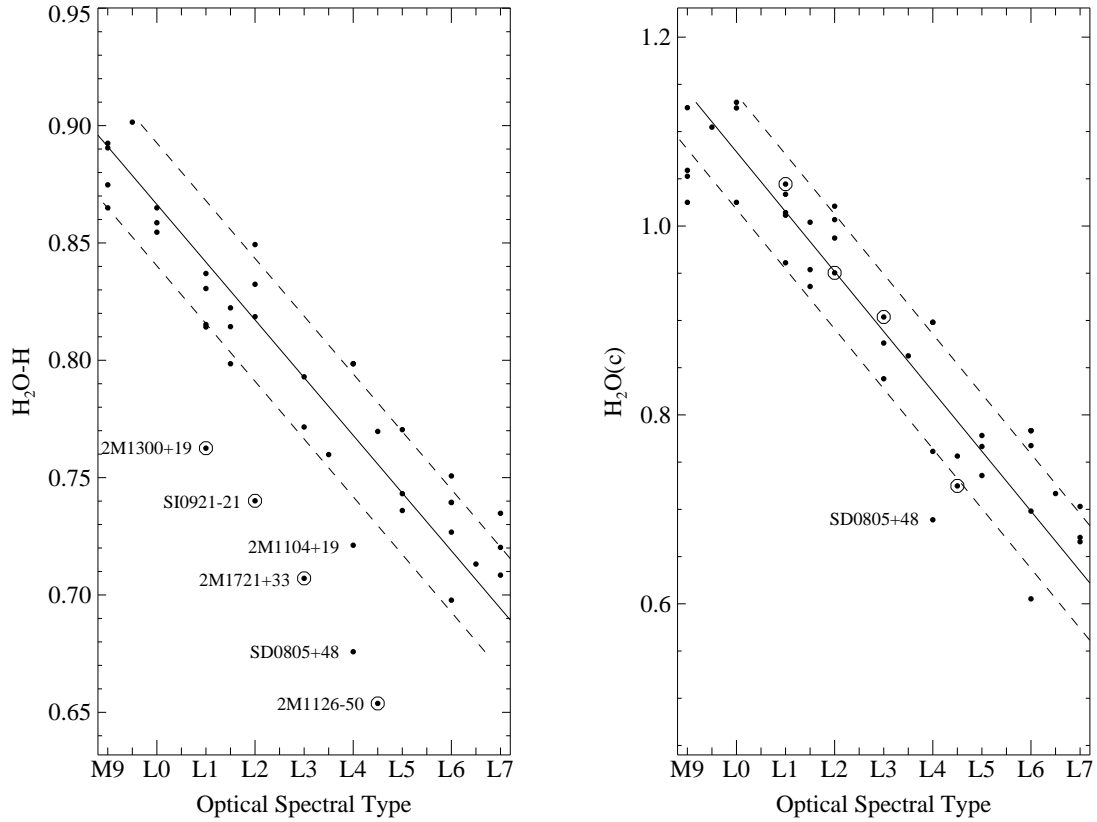


FIG. 11.— Values for the $1.4 \mu\text{m}$ H_2O spectral ratios $\text{H}_2\text{O-H}$ (left) and $\text{H}_2\text{O(c)}$ (right) as a function of optical spectral type for 39 unresolved, non-peculiar and optically classified field late-M and L dwarfs (dots) and the four blue L dwarfs in Figure 5 (circled dots). Linear fits for the normal field dwarfs are indicated by solid lines, with dashed lines indicating 1σ scatter (roughly 1 subtype). The blue L dwarfs clearly stand out in the left panel due to their enhanced $1.4 \mu\text{m}$ H_2O absorption, while the color-corrected $\text{H}_2\text{O(c)}$ ratio yields subtypes consistent with their optical types within the scatter. The additional L4 outliers in the left panel are SDSS J080531.84+481233.0 (Hawley et al. 2002; Knapp et al. 2004) and 2MASS J11040127+1959217 (Cruz et al. 2003), which have also have blue $J - K_s$ colors. The former may be an unresolved binary (Burgasser 2007b).

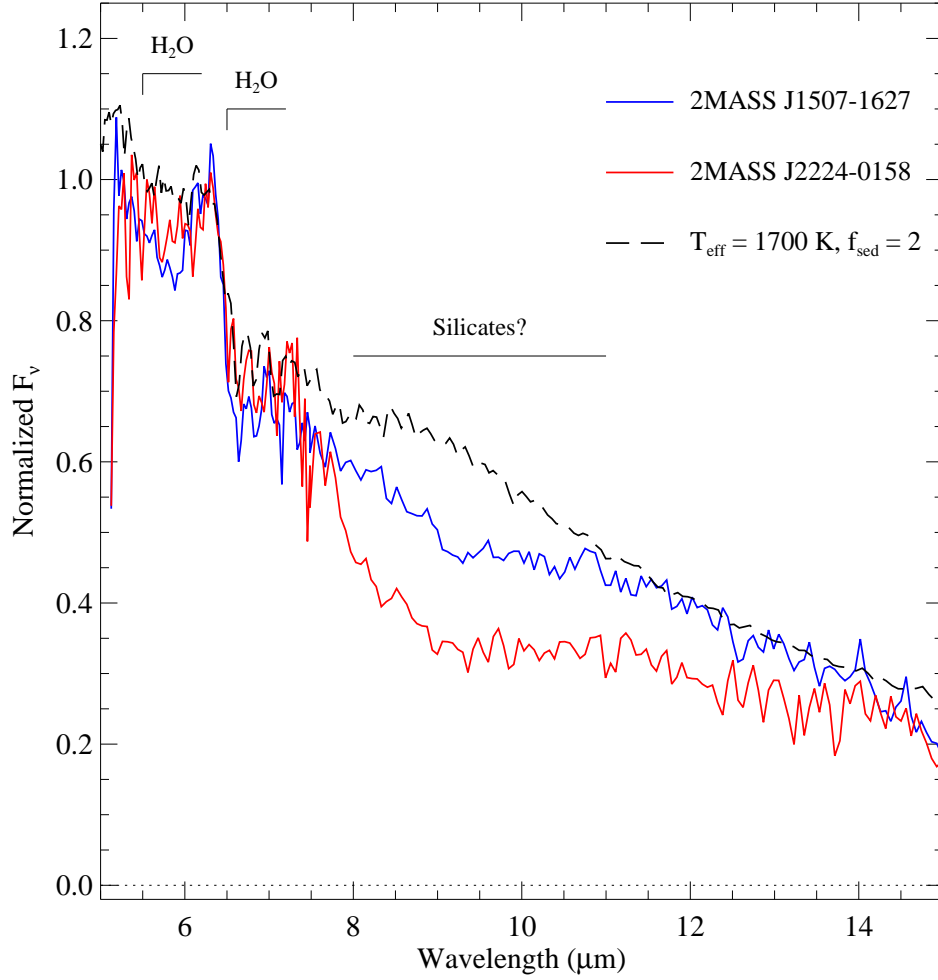


FIG. 12.— Mid-infrared spectra obtained with the *Spitzer* Infrared Spectrograph (Houck et al. 2004) of the L dwarfs 2MASS J2224-0158 (L4.5; red line) and 2MASS J1507-1627 (L5; blue line) from Cushing et al. (2006). These sources are ~ 0.2 – 0.3 mag bluer and redder in $J - K_s$ than the average midtype L dwarf, respectively (Kirkpatrick et al. 2000). A broad absorption feature apparently present in the 8–11 μm region of both spectra has been tentatively identified as arising from the Si-O stretch mode associated with condensate species. This feature is clearly weaker in the bluer and possibly less cloudy L dwarf 2MASS J1507-1627. Also shown is a $T_{\text{eff}} = 1700 \text{ K}$, $\log g = 5.0$, $f_{\text{sed}} = 2$ spectral model from M. Marley et al. (in preparation.) that does not exhibit this feature (see discussion in Cushing et al. 2006). All spectra are normalized at 6.4 μm .